Asymptotic densities for Packard *Box* rules

Janko Gravner
Mathematics Department
University of California
Davis, CA 95616
e-mail: gravner@math.ucdavis.edu

David Griffeath
Department of Mathematics
University of Wisconsin
Madison, WI 53706
e-mail: griffeat@math.wisc.edu

(Revised version, February 2009)

Abstract. This paper studies two-dimensional totalistic solidification cellular automata with Moore neighborhood such that a single occupied neighbor is sufficient for a site to join the occupied set. We focus on asymptotic density of the final configuration, obtaining rigorous results mainly in cases with an additive component. When sites with two occupied neighbors also solidify, additivity yields a comprehensive result for general finite initial sets. In particular, the density is independent of the seed. More generally, analysis is restricted to special initializations, cases with density 1, and various experimental findings. In the case that requires either one or three occupied neighbors for solidification, we show that different seeds may produce many different densities. For each of two particularly common densities we present a scheme that recognizes a seed in its domain of attraction.

2000 *Mathematics Subject Classification*. Primary 37B15. Secondary 68Q80, 11B05.

Keywords: additive dynamics, asymptotic density, cellular automaton, growth model.

Acknowledgments. Experimental aspects of this research were conducted by a Collaborative Undergraduate Research Lab (CURL) at the University of Wisconsin-Madison Mathematics Department during the 2006–7 academic year. The CURL was sponsored by a National Science Foundation VIGRE award. We are particularly grateful to lab participants Charles D. Brummitt and Chad Koch for empirical analysis of the *Box 12* rule.

Support. JG was partially supported by NSF grant DMS–0204376 and the Republic of Slovenia's Ministry of Science program P1-285. DG was partially supported by NSF grant DMS–0204018.

1 Introduction

In 1984, a family of very simple and intriguing cellular automata (CA) were introduced by Packard [**Pac**] as prototypes for snow crystal formation. These growth models were subsequently studied experimentally [**PW**], and popularized by Wolfram [**Wol1**], who has used them ever since to illustrate two principal tenets of his research approach: (*i*) simple CA rules capture the essential features of many complex physical phenomena, but (*ii*) they are largely beyond the purview of rigorous mathematics and so best studied by computer simulation. Indeed, identification of exact global asymptotics for nontrivial local interactions is rare in cellular automata, or other nonlinear spatial dynamics. Nevertheless, in [**GG1**] we were able to prove that, starting from a singleton, a two-dimensional Packard rule — *Box 1* in the terminology introduced in the sequel — fills the lattice with asymptotic density 4/9. The present paper is the third in a subsequent series devoted to mathematical study of Packard snowflake cellular automata on the simplest neighborhoods of the two-dimensional integer lattice. Quite complete analyses of the hexagonal and diamond neighborhood settings appear in [**GG2**] and [**BDR**], respectively. Here we address the much more challenging box neighborhood family, four examples of which are pictured on p. 373 of [**Wol2**]. We view Packard's CA models as beautiful algorithms that grow lattice crystals delicately perched between pattern and complexity, and like the celebrated early fractal known as the Koch snowflake, are of interest in their own right. Regarding verisimilitude, in two recent modeling papers [**GG3**, **GG4**] we argue that physical snow crystals are governed by diffusion-limited growth with anisotropic attachment, so the development of real planar snowflakes such as sectored plates and dendrites is emulated by Packard's rules only at a rather superficial level.

Whereas Packard snowflakes *are* amenable to rigorous mathematics, it would be nearly impossible to understand their behavior without the aid of interactive simulation and visualization software. We wish to single out two programs that were indispensable for our study: *MCell* [**Woj**] and *Golly* [**TR**]. The former is a superb, general-purpose CA experimentation platform; the latter supports only a much more limited rule set, but handles gigantic arrays with remarkable speed. We have provided numerous helpful figures throughout the paper to illustrate key aspects of our analysis, but readers will surely require some such simulation tool to accompany a careful reading. That said, let us now proceed with the formal framework for our study.

We consider a class of two-dimensional binary CA. A *configuration* is thus a member of $\{0,1\}^{\mathbb{Z}^2}$: at each time, any site in the two-dimensional lattice $\mathbb{Z}^2$ is in one of two states, 0 or 1. This divides the lattice into two sets, the *occupied* sites in state 1, and the *empty* sites in state 0.

Our CA rules *solidify*: the set of occupied sites increases in discrete time, with its evolution given by $A_0 \subset A_1 \subset A_2 \subset \cdots \subset \mathbb{Z}^2$. Every solidification rule has a well-defined *final set* $A_\infty = \cup_{n\geq 0} A_n$. Our rules are also *totalistic*. Such a rule is, in general, specified by the following two ingredients. The first is a finite *neighborhood* $\mathcal{N} \subset \mathbb{Z}^2$ of the origin, its translate $z + \mathcal{N}$ then being the neighborhood of point z. The second ingredient is a *solidification list* S of neighborhood counts that result in occupation at the next time. We represent S as a subset of $\{1, \ldots, 8\}$, or as a string comprising its elements in increasing order, as convenient. Formally,

then, if $z \notin A_t$, then $z \in A_{t+1}$ iff $|(z + \mathcal{N}) \cap A_t| \in S$.

We will only discuss CA with three simple neighborhoods: *Diamond* rules with von Neumann neighborhood $\mathcal{N} = \{(0,0),(0,\pm1),(\pm1,0)\}$, *Box* rules with Moore neighborhood $\mathcal{N} = \{(0,0),(0,\pm1),(\pm1,0)\},(\pm1,\pm1)\}$ and *Hex* rules with the neighborhood $\mathcal{N} = \{(0,0),(\pm1,0),(0,\pm1),\ \pm(1,1)\}$. For example, in *Box 1357*, a 0 turns into a 1 exactly when it "sees" an odd number of already occupied neighbors in its Moore neighborhood.

The canonical finite initial configuration, or *seed*, is a single occupied site at the origin, $A_0 = \{0\}$, but we will also be interested in arbitrary *finite* initial states (i.e., those that contain only finitely many occupied sites). Infinite initial states such as lines and wedges will also enter into several proofs.

Our principal object of study is the density of the final set A_∞. Let μ_ϵ be ϵ^2 times the counting measure on $\epsilon \cdot A_\infty$. We say that A_∞ has *density* ρ if μ_ϵ converges to $\rho \cdot \lambda$ as $\epsilon \to 0$. Here λ is Lebesgue measure on $\mathbb{R}^2$ and convergence holds in the weak-* sense:

$$\int f\, d\mu_\epsilon \to \rho \cdot \int f\, d\lambda \ , \tag{1}$$

for any $f \in \mathcal{C}_c(\mathbb{R}^2)$. Equivalently, for any square $R \subset \mathbb{R}^2$, the quantity $\epsilon^2 \cdot |R \cap (\epsilon \cdot A_\infty)|$ converges to $\rho \cdot \mathrm{area}(R)$ as $\epsilon \to 0$.

We will assume that 1 is in the solidification list S, for otherwise the analysis quickly becomes too difficult [**GG1**]. Such rules are often referred to as *Packard snowflakes* [**Pac**, **PW**, **TM**, **GG1**, **GG2**, **BDR**, **Wol2**]. In the *Diamond* and *Hex* cases we may also assume $2 \notin S$, or the density is easily shown to be 1. The resulting four *Diamond* and sixteen *Hex* cases then all have well-defined densities that are independent of the seeds [**GG2**, **BDR**]. These densities are rational and can be computed exactly for all *Diamond* and eight of the *Hex* cases (namely *13, 135, 134, 1345, 136, 1356, 1346*, and *13456*). The remaining eight *Hex* cases all have densities that are nontrivial (i.e., different from 0 or 1), not known exactly, but can be approximated quite accurately [**GG2**].

This paper is devoted to investigation of density issues for the 128 *Box* Packard snowflakes. It has been known for a while that there is no hope of a complete analysis as in the *Hex* and *Diamond* settings. For instance, under the *Box 1* rule different seeds may result in different densities. Namely, it is shown in [**GG1**] that a singleton yields a replicating structure with density 4/9, whereas D. Hickerson (private communication) engineered finite seeds that generate essentially periodic crystals with densities 29/64 and 61/128. The latter is achieved by an ingenious arrangement of 180 occupied cells strategically placed around the boundary of an 83×83 grid. Not much more is known rigorously about this rule, although experiments suggest that most seeds generate chaotic growth with a density around 0.51.

The one straightforward *Box* case consists of rules with $\{1,2,3\} \subset S$. It is an easy exercise to prove that, starting from any finite A_0, such rules eventually occupy every site more than distance $d = d(A_0)$ from $\{(x,y) : y = \pm x\}$, and thus have density 1.

The fundamental tool used to prove *Diamond* and *Hex* results is an additive component that creates an impenetrable *web* of occupied cells [**GG2**]. This web consists of occupied sites

at the edge of the "light cone," or more precisely, sites that solidify at a time equal to the graph-theoretic distance from the seed. Here the *neighborhood graph* consists of sites $z \in \mathbb{Z}^2$ and edges between z_1 and z_2 with $z_2 - z_1 \in \mathcal{N}$. We call the rule that governs occupation of such sites the *extreme boundary dynamics (EBD)*.

For our purposes, an *additive* dynamics is a one-dimensional CA rule with states 0 and 1 that preserves addition modulo 2. As *the* basic tool, additivity plays the role of linearity in continuous dynamical systems. The prime example of an additive rule is ℓ_t, considered in Section 3, for which $\ell_t(x) = \ell_{t-1}(x) + \ell_{t-1}(x-1) \mod 2$ (see [**GG2**] for an introduction and some references). The EBD for *Hex* and *Diamond* Packard snowflakes are easily seen to be equivalent to ℓ_t.

For *Box* rules, the sides of the neighborhood have three cells, so a priori one would expect the dynamics easiest to analyze to be *Box 13*. Indeed, this rule does have additive EBD $\bar{\ell}_t$, given by $\bar{\ell}_t(x) = \bar{\ell}_{t-1}(x+1) + \bar{\ell}_{t-1}(x) + \bar{\ell}_{t-1}(x-1) \mod 2$. However, as we will see in Section 7, the resulting web "leaks," seeds amenable to rigorous analysis are greatly restricted, and the general behavior is similar to that of *Box 1*, which has a non-additive EBD.

Rather, the most tractable case turns out to be *Box 12*. At first this seems surprising, since its EBD is *not* additive. However, it does emulate additive dynamics in essential aspects [**Jen1**, **Jen2**]. (We note in passing that in the CA literature, versions of the *Box 13* and *Box 12* EBD are often referred to as Rule 150 and Rule 126, respectively.) Thus the web is sufficiently well-behaved to yield Theorem 1, a general result covering the 32 rules with 1 and 2, but not 3, on the solidification list. These cases are divided into two groups because of different proofs and different rates of convergence to the asymptotic density. The two groups also have different macroscopic dynamics — we will not discuss this concept in detail here (see [**GG2**]), but one can readily get the basic idea from Figure 1.

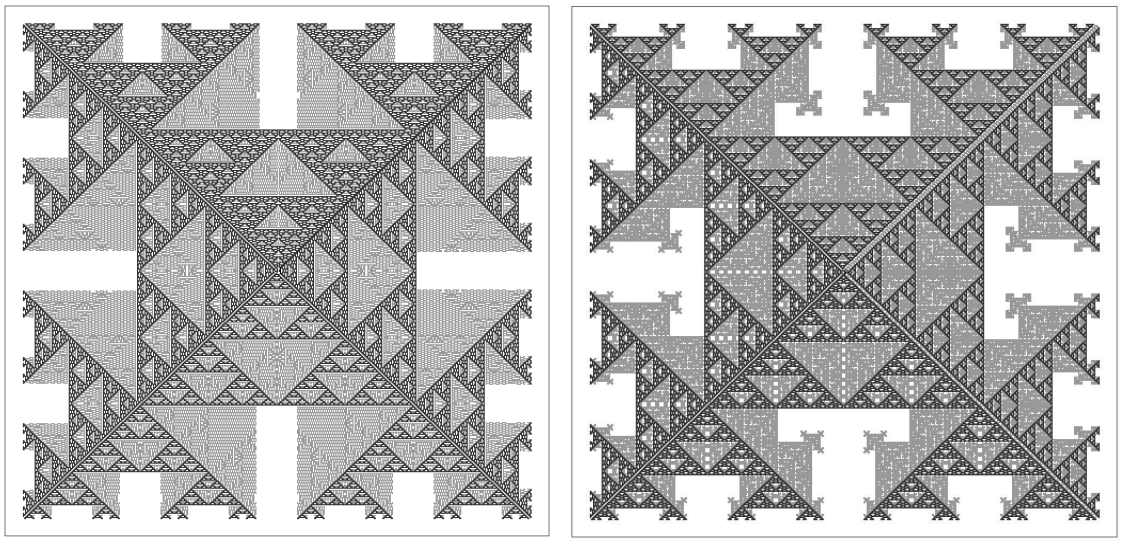

Fig. 1. *Box 12* (left) and *Box 124* (right) rules, each started from a (different) random subset of a 7×7 box. Both dynamics are depicted at time 235 and have the EBD highlighted.

As is apparent from these snapshots, each EBD generates, in each of the four coordinate directions, a replicating structure similar to (in fact, a bounded perturbation of) the Sierpinski lattice, that is, Pascal's Triangle modulo 2 (see Lemma 2.4). The large-scale limit of this web is a fractal with Hausdorff dimension $\log 3/\log 2 < 2$; thus it contributes nothing to the asymptotic density of occupied sites. However, as suggested by Figure 1, triangular regions enclosed by the web are subsequently filled with nearly uniform patterns generated by the *Box* CA subject to boundary conditions imposed by the boundaries of the triangles. These dynamics have their own internal EBD, which generates a secondary web. In the *Box 12* case, but not in the *Box 124* case, this secondary web is significantly different from the Sierpinski lattice. In either instance, this induces further division into subdomains, which are further subdivided, and so on. The key fact is that the number of domain types is finite, inducing a finite alphabet of nested CA with boundaries (see Figures 2–5 and Figure 8). Thus the density ρ can be determined explicitly by a linear recursion and the proportion of sites in A_∞ is close to ρ within sufficiently large domains. Lastly, from the macroscopic perspective, the subdivision can be made arbitrarily fine, which ensures uniformity of the resulting density across space (see Section 5 for more details).

Theorem 1. *Consider Box rules with* $1 \in S$, $2 \in S$, $3 \notin S$. *All these have densities that are independent of the seed.*

Group I. The density of Box 12 is $2/3$. *The density is also* $2/3$ *for the other seven rules with* $4 \notin S$ *and* $7 \notin S$. *For the eight rules such that* $4 \notin S$ *and* $7 \in S$, *the density is 1. The density is also 1 for the eight rules with* $\{4, 5\} \subset S$.

Group II. Box rules 12467 and 124678 have density 1. The remaining 6 cases, 124, 1248, 1247, 12478, 1246, and 12468, have 6 distinct nontrivial densities given in Table 1.

Table 1 also displays formulas for the population counts, starting from the 2×2 box $[0, 1]^2$, at the fixation time on the box $[-(2^n - 1), 2^n]^2$. It will become clear in Section 2 why a 2×2 box is the natural seed for the rules of Theorem 1.

rule	density	no. of sites in $[-(2^n-1), 2^n]^2$	time	validity
124	$65/72 \approx .9027$	$(65/18)\,4^n + 2 \cdot 2^n + (8/3)\,n - 64/9$	$2^n - 1$	$n \geq 2$
1248	$269/288 \approx .9340$	$(269/72)\,4^n + 2 \cdot 2^n + (8/3)\,n - 64/9$	2^n	$n \geq 3$
1247	$89/96 \approx .9271$	$(89/24)\,4^n + 8 \cdot n - 40/3$	2^n	$n \geq 3$
12478	$23/24 \approx .9583$	$(23/6)\,4^n + 8 \cdot n - 40/3$	2^n	$n \geq 2$
1246	$139/144 \approx .9653$	$(139/36)\,4^n + 2 \cdot 2^n + 16/3\,n + 80/9$	2^n	$n \geq 3$
12468	$35/36 \approx .9722$	$(35/9)\,4^n + 2 \cdot 2^n - (32/3)\,n + 208/9$	$2^n + 1$	$n \geq 3$

Table 1. Six *Box* rules with nontrivial densities different from 2/3.

Sections 2–6 are devoted to the analysis of the EBD for rules covered by Theorem 1, and other details of the proof. Using the EBD and its connection to the additive rule ℓ_t, Sections 2–4 analyze the behavior of *Box 12* on different types of web domain; then Section 5 proves Theorem 1 for Group I, and Section 6 describes the modifications of the argument needed to handle Group II. In contrast, *Box 13* requires analysis of a more complex *two-level EBD* $\bar{\ell}_t^2$, an extension of $\bar{\ell}_t$ that is no longer additive. These dynamics are introduced in Section 7, where it

is shown that there exist seeds from which $\bar{\ell}_t^2$ behaves as if it were additive, due to an emergent structure known as a *replicator*. Even for these, though, the density is not always the same: we present examples with densities 1/2, 28/45, 5/8, 21/32, and 3/4. For each of the first two densities we devise an algorithm that determines whether a seed is in its domain of attraction. *Box 13* is also apparently capable of complex growth, about which we are unable to say anything rigorous.

Finally, Section 8 provides an overview of the remaining Packard snowflakes: rules with $2 \notin S$ but $i \in S$ for some $i \geq 4$. Rigorous results are harder to come by in these cases; indeed, many of them seem intractable. Nevertheless, just as for *Box 13*, additive structure emerges in the form of a replicator for some rules and special seeds. For instance, we identify twelve additional Packard snowflakes with a computable nontrivial density starting from a singleton. It is also possible to prove that some of the remaining rules have density 1. We present two particularly interesting examples: *Box 145678*, which we analyze by comparison with a critical threshold growth CA [**GG1**]; and *Box* rules with $\{1, 3, 4, 5\} \subset S$, which are controlled by extending the EBD to three levels in some situations.

2 Jen's conjugacy for the extreme boundary dynamics of *Box 12*

The key concept in our proof of Theorem 1 is the *extreme boundary dynamics (EBD)* B_t, a solidification CA with neighborhood of $z \in \mathbb{Z}^2$ given by $z + \{(-1,-1),(0,-1),(1,-1)\}$ and the rule that requires an empty site to have one or two occupied sites in its neighborhood to become occupied. We will assume the initial state B_0 is a subset of the x-axis. A closely-related formulation represents the EBD as a one-dimensional CA, with neighborhood of $x \in \mathbb{Z}$ given by $\{x-1, x, x+1\}$ and rule b_t such that $b_t(x) = 1$ iff there are one or two 1's in the set $\{b_{t-1}(x-1), b_{t-1}(x), b_{t-1}(x+1)\}$. Here B_t is the space-time representation of b_t. As is customary, we render the y-axis of time directed *downward* when depicting the evolution of B_t.

The connection between A_t and B_t is simple but very useful. Namely, if $A_0 \subset \{(x,y) : y \leq 0\}$ and B_0 is the intersection of A_0 with the x-axis, then sites that become occupied at time t on the line $y = t$ are the same:

$$A_t \cap \{y = t\} = B_t \cap \{y = t\} = B_t \setminus B_{t-1}. \tag{1}$$

Our first version of *additive* dynamics is the symmetric one, denoted by L'_t: the solidification CA with neighborhood of $z \in \mathbb{Z}^2$ given by $z + \{(-1,-1),(1,-1)\}$ and the rule in which a 0 site requires exactly one occupied site in its neighborhood to change to 1. Its one-dimensional counterpart is denoted ℓ'_t.

In each case, to emphasize a seed we put it in a superscript, e.g., b_t^Λ starts from the set Λ. We wish to emphasize that in this section all configurations live on the infinite line, so there are no boundary conditions.

Following [**Jen1**, **Jen2**], we begin study of the EBD by dividing its one-dimensional state into maximal contiguous blocks of single type (0 or 1). *Odd* and *even* blocks consist of odd

and even numbers of sites, respectively, and we also call any infinite block even. The next three lemmas are from [**Jen1**].

Lemma 2.1. *If all blocks are initially even, then under either b_t or ℓ'_t they stay so forever and the two dynamics agree.*

A useful observation is that L'_t induces two independent dynamics, one on odd sites (those that have sum of coordinates odd) and one on even sites. If all blocks are even the two have identical initial states, and one may reduce each block by a factor of two and the dynamics to the irreducible version L_t considered in the next section.

Lemma 2.2. *If the number of odd blocks is initially finite, then under b_t it is nonincreasing in time.*

Define *Jen's conjugacy map* $J(\Lambda)$ on a configuration Λ by inserting a site of the same type into any odd block.

Lemma 2.3. *Provided that the number of odd blocks is finite and constant on some time interval* $[t_1, t_2]$,

$$J(b_t^\Lambda) = b_t^{J(\Lambda)}, \qquad t \in [t_1, t_2].$$

In fact, as also pointed out in [**Jen1**], the odd blocks can be tracked through time so that each has a well-defined successor unless it gets annihilated by another odd block. As the description in [**Jen1**] is a bit difficult to parse, we provide a few more details.

An odd block of 0's of size at least 3 shrinks by 1 from each of its ends and this is its successor. An odd block of 1's of size at least 3 turns into a block of 0's, also shrunk by one from both ends, again defining the successor.

An isolated 0 must turn into a 1, which is part of some block of 1's that is the successor in this case. To find the left edge of the block, one moves leftward from the isolated 0 to the first block B_L of size at least 3; the rightmost site of B_L is then the position of the leftmost 1 of the successor block of 1's. The rightmost 1 in the successor block is determined analogously. It is easy to check that the described successor is odd iff the number of odd blocks it succeeds is itself odd. In this sense, the odd blocks annihilate in pairs, which is the only mechanism for their number to decrease.

An isolated 1 can only arise initially (as a little case checking demonstrates), when its successor is defined in the same way as in the case of an isolated 0. Also note that, from the construction, an odd block of 1's is at strictly positive times always succeeded by a block of 0's. Odd blocks of 0's are then eventually succeeded by singletons.

The final result of this section establishes that, from general seeds, the behavior of b_t emulates the behavior of ℓ'_t. This lemma is the key step in proving that the density of any rule with $1, 2 \in S$ but $3 \notin S$ does not depend on the finite initializations.

Lemma 2.4. *Given any (finite) seed Λ, there exists a finite set $\Lambda_0 = \Lambda_0(\Lambda)$ with only even blocks and an $n_0 = n_0(\Lambda)$ so that at times $n_0 + 2^n$, $n \geq n_0$, the state of b_t^Λ consists of two copies*

of Λ_0. *The interval* $[a_n, b_n]$ *of 0's between two copies may have an odd or an even number of 0's, agreeing with the parity of odd blocks in* Λ. *Moreover, there exist integers* $D_n \geq 1$, *uniformly bounded by a constant that depends only on* Λ, *such that the block* $[a_n, b_n]$ *is the last in the chain of successors starting with the block* $[a_n - D_n, b_n + D_n]$ *of* 1*'s, and continuing with blocks* $[a_n - D_n + i, b_n + D_n - i]$ *of* 0*'s,* $i = 1, \ldots, D_n$.

Proof. From some time on, the number of odd blocks must be constant. Without loss of generality, we may assume that this is already true initially. We will later prove that this constant number of odd blocks must be 0 or 1, but do not assume so at this point.

Fix an odd block in Λ and track its successor singleton 0's, say $(x_1, t_1), (x_2, t_2), \ldots$ We claim that

$$x_{k+1} - x_k \leq t_{k+1} - t_k - 2. \tag{2}$$

To show this, assume without loss of generality that $k = 1$ and $(x_1, t_1) = (0, 0)$. Let the successor of the isolated 0 at $(0, 0)$ be block $[a, b]$, where $b - a + 1$ is odd. It is easy to check that $a \leq -1$, and that

$$(x_2, t_2) = (a + (b - a)/2, 1 + (b - a)/2),$$

which establishes the claim immediately. As an illustration, consider the following example in which the isolated 0's are in bold, and the successor of the first isolated 0 has seven 1's and is positioned as far to the right as possible:

	1	**0**	1					
0	1	1	1	1	1	1	1	0
	1	0	0	0	0	0	1	
		1	0	0	0	1		
			1	**0**	1			

By symmetry, it must also be true that

$$x_{k+1} - x_k > -(t_{k+1} - t_k). \tag{3}$$

We claim that, at times 2^n, for a large enough n, Jen's conjugacy guarantees that the state b_t^Λ consists of two finite sets, both at most twice the length of Λ, separated by a long interval of 0's.

To see this, first recall that ℓ'_t *replicates* [**Wil1**, **Wil2**, **GG1**]. Namely, started from any finite set, the state at sufficiently large time 2^n consists of two copies of the initial set separated by 0's. This property of ℓ'_t, together with Lemma 2.1, guarantees that $b_t^{J(\Lambda)}$ consists of two translates of $J(\Lambda)$ (which has length at most twice the length of Λ), separated by an interval of 0's. This is, by Lemma 2.3, also the configuration $J(b_t^\Lambda)$, and therefore b_t^Λ is obtained by removing at most a site from each block of $b_t^{J(\Lambda)}$, which proves the claim from the previous paragraph.

Moreover, the rightmost 1 in b_t^Λ moves at the "speed of light," i.e., one step to the right at each time unit. It follows from the claim above, together with (2) and (3), that any isolated 0

(which by our assumption cannot be annihilated) must have the described long middle interval as its successor. Hence this interval is the sole possibility for a remaining odd interval, if indeed any does remain. Let the first time this happens define n_0, and let Λ_0 be either of the two finite sets.

If no odd blocks remain at time 2^{n_0}, then the dynamics is ℓ'_t thereafter and there is nothing left to prove. Otherwise, we use Lemma 2.3 again: at times $t = 2^n$, $n \geq n_0$, we obtain b_t^Λ by removing the middle 0 from $\ell_t'^{J(\Lambda)}$. But this last configuration consists of two copies of Λ_0, separated by 0's.

To prove the last assertion of the lemma, consider the configuration at the previous time. If the state of $a_n - 1$ is 1, then the entire interval $[a_n - 1, b_n + 1]$ must consist of 1's, there are 0's at $a_n - 2$ and $b_n + 2$, and $D_n = 1$. Otherwise, if the state of $a_n - 1$ is 0, then the entire interval $[a_n - 1, b_n + 1]$ must consist of 0's, and the states of $a_n - 2$ and $b_n + 2$ are 1. Continuing backwards in time, the second possibility can occur only finitely many times, since Λ_0 is finite and the leftmost (resp. rightmost) 1 moves by one unit to the left (resp. to the right) at each time. □

3 Facts about additive dynamics

In this section we deal with an asymmetric version L_t of additive dynamics that is equivalent but irreducible (in the sense that $\mathbb{Z} \times \{0, 1, 2 \dots\}$ cannot be divided into two sets on which L_t operates independently), and notationally more convenient. The rule is the same as L'_t, except the neighborhood of $z \in \mathbb{Z}^2$ is $z + \{(-1, -1), (0, -1)\}$. Again, the one-dimensional variant is ℓ_t.

We begin with a simple observation that is one of the key reasons why the asymptotic density of *Box 12* equals 2/3. Consider the initial state $I_0 = \dots 11011\underline{0}11011 \dots$. Here, and in the sequel, the position of the point with x-coordinate 0 is underlined. Keeping in mind the interpretation of a configuration I as the set of 1's in I, we denote the *translation* (also known as *shift*) of I by x as $I + x$.

Lemma 3.1. *The additive dynamics ℓ_t translates I_0 two units to the right.*

Let us next consider a one-sided version of I_0:

$$I_1 = \dots 0110110110\underline{1}00000000 \dots$$

Lemma 3.2. *At times $t_n = 2^n$, $n = 0, 1, 2, \dots$, the configurations $\ell_{t_n}^{I_1}$ and $I_1 + t_n$ agree on strictly positive sites. On nonpositive sites, $\ell_t^{I_1}$ and $I_1 + 2t$ agree for all $t \geq 0$.*

Proof. The last statement follows from the previous lemma, so we proceed to the proof of the first claim. At time t_n, the state of $\ell_{t_n}^{\{0\}}$ consists of exactly two occupied sites, at 0 and at t_n; call this configuration R_n. By additivity

$$\ell_{t_n}^{I_1} = \sum_{x \in I_1} (x + R_n) \mod 2.$$

On strictly positive sites, this is the same as

$$\sum_{x \in I_1} (x + t_n) = I_1 + t_n.$$

□

The next initial state is a perturbation of I_0 with a 0 taken out:

$$I_2 = \ldots 011011011\underline{1}10110110\ldots$$

Lemma 3.3. *At times $t_n = 2^n - 2$, n odd, $\ell_{t_n}^{I_2}$ is*

$$\ldots 011011011\underline{\mathbf{1}}\mathbf{11}\ldots\mathbf{1}110110\ldots,$$

where the bold segment consists of $2^n - 2$ 1's.

Proof. Note that $t_n = 0 \mod 3$. Also note that, modulo 2,

$$I_2 = I_0 + I_1',$$

where

$$I_1' = \ldots 0000\underline{1}0110110\ldots$$

is the reflection of I_1. At time t_n, $\ell_{t_n}^{\{0\}}$ is the finite configuration

$$\underline{1}010101\ldots 1,$$

with the last 1 at site t_n. By additivity

$$\ell_{t_n}^{I_2} = \ell_{t_n}^{I_0} + \sum_{x \in I_1'} (\ell_{t_n}^{\{0\}} + x) \mod 2,$$

and the second term is on $[0, 2^n - 3]$ the sum, modulo 2, of

$$\begin{aligned} \underline{\mathbf{1}}0101010\ldots 0 \\ 101010\ldots 0 \\ \mathbf{1}0101\ldots 1 \\ 101\ldots 1 \\ \mathbf{1}0\ldots 0 \\ \ldots \end{aligned}$$

The bold entries mark which column sums are odd, so the result is, on $[0, 2^n - 3]$,

$$\underline{1}001001\ldots 0$$

This we need to add to

$$\ell_{t_n}^{I_0} = \ldots 011\underline{0}11011011\ldots,$$

to get the claimed result on the bold interval. Elsewhere, the result is not influenced by the perturbation, and follows from Lemma 3.1. □

Lemma 3.4. *At times $t_n = 2^n$, n even, $\ell_{t_n}^{I_2}$ is*

$$\ldots 11011011\underline{\mathbf{0}}\mathbf{11011}\ldots\mathbf{110}011011\ldots,$$

where the bold portion of the invariant state consists of 2^n sites.

Proof. Now $t_n = 1 \mod 3$. As in the proof of Lemma 3.2, $\ell_{t_n}^{\{0\}} = R_n$, and now

$$\ell_{t_n}^{I_0} = \ldots 0110\underline{1}10110110\ldots.$$

To compute the state on the bold interval, we therefore need only add I_1', which is easily checked to give the claimed result. Again, Lemma 3.1 handles sites outside the bold interval. □

The final perturbation of I_0 we will need has an added 0 at the origin:

$$I_3 = \ldots 1101101100110110110\ldots,$$

The proofs of our last two lemmas in this section are easy adaptations of the previous two proofs.

Lemma 3.5. *At times $t_n = 2^n - 2$, n even, $\ell_{t_n}^{I_3}$ is*

$$\ldots 011011011\underline{\mathbf{1}}\mathbf{11}\ldots\mathbf{1}110110\ldots,$$

where the bold segment consists of $2^n - 2$ 1's.

Lemma 3.6. *At times $t_n = 2^n$, n odd, $\ell_{t_n}^{I_3}$ is*

$$\ldots 011011011\underline{\mathbf{1}}\mathbf{10110}\ldots\mathbf{011}110110\ldots,$$

where the bold portion of the invariant state consists of 2^n sites.

4 *Box 12* in a wedge

In this section we analyze the *Box 12* rule A_t with various initial conditions. These correspond to the finite alphabet of boundary conditions under which A_t recursively occupies its web domains. The recursion is established by Lemmas 4.2–4.5. Throughout, we exploit the associated EBD B_t: whenever the initial state has no odd blocks (or their position is sufficiently remote) we may, by Lemma 2.1, use the results of Section 3, as indeed we do in every proof. To begin, note that the initial state I_4 with 0's off the x-axis, and

$$\ldots 00111100111\underline{0}0111100\ldots$$

on the x-axis, is translated three units (the two horizontal directions are equivalent) by b_t, as follows from Lemma 3.1 (since b_t may be thought of as two independent copies of ℓ_t acting on alternating sites), or by an easy direct verification. Hence all sites with positive y-coordinate that are ever occupied by A_t are actually occupied by B_t, since all empty sites on the line $y = t$, between the "bricks" laid by B_t, see four 1's at that time and seven 1's thereafter.

Our next initial states I_5^i, $i = 1, 2, 3, 4$, are 0 everywhere, except for 1's on $\{(-1, y) : y \in \mathbb{Z}\}$, and the following configurations on the nonnegative part of the x-axis:

$$\underline{0}10111100111110011111001\ldots \quad (I_5^1),$$
$$\underline{0}11100111100111100111\ldots \quad (I_5^2)$$
$$\underline{0}10011110011110011110 0\ldots \quad (I_5^3)$$
$$\underline{0}11110011110011110011\ldots \quad (I_5^4)$$

The 1's on the y-axis in I_5^i, as well as in I_6 below, have the role of boundary conditions. To ensure the proper web analogue of (1), we introduce a *modified* EBD $\tilde{B}_t$, which uses the same rule as B_t to decide the occupation of sites with strictly positive x-coordinate; whereas, at location $(0, t)$ and at time $t > 0$, the occupation is decided by A_t. The rule $\tilde{B}_t$, unlike B_t, leaves all the sites $(0, t)$, $t > 0$, unoccupied.

Lemma 4.1. *Starting from I_5^1, $\tilde{B}_1$ has configuration I_5^2 on the nonnegative part of $\{y = 1\}$, and vice versa. The same relationship holds between I_5^3 and I_5^4. In every case, all sites with positive y-coordinate that are ever occupied by A_t are occupied by $\tilde{B}_t$.*

Proof. Direct verification. □

Less straightforward is the initial state I_6 with the origin and the vertical line to its left $\{(-1, y) : y \in \mathbb{Z}\}$ initially occupied. We define final occupation counts in the wedge:

$$\beta_n = |A_\infty \cap \{(x, y) : 1 \le y \le 2^n, 1 \le x \le y\}|.$$

For instance, this sequence begins with $1, 3, 9, 30, 105, 392, \ldots$. (We will not enumerate further wedge counts in this section, but will ultimately derive an exact recursion that generates them.)

Lemma 4.2. *Starting from I_6, $\tilde{B}_1$ occupies (1,1) and, for $t \ge 2$, $\tilde{B}_t$ and A_t occupy at least $(1, t)$, $(t - 1, t)$ and (t, t). Moreover, at time 2^n, $n \ge 2$, the configuration of both $\tilde{B}_t$ and A_t on the interval $\{(x, 2^n) : x \in [0, 2^n]\}$ is one of the following:*

$$\underline{0}1011110011110011111\ldots 0011110011 \quad (n \text{ even})$$
$$\underline{0}1111001111001111 0\ldots 0011110011 \quad (n \text{ odd})$$

In particular, $\tilde{B}_t$ completely seals the wedge — that is, the set in the definition of β_n — at time $2^n + 1$, in the sense that it creates an impenetrable boundary so nothing outside can ever influence the dynamics, and thus the occupation count, inside.

Proof. The reader may consult Figure 2, in which black sites represent I_6 and dark grey sites $\tilde{B}_t$. The claim in the first sentence is easily proved by induction. Inductive argument works for the claim in the second sentence as well. The $n = 2$ case can be easily checked. To verify the $n - 1 \to n$ claim, one uses a speed of light argument:

- all sites $(x, 2^{n-1} + k)$, $x \le 2^{n-1} - k$ at time $2^{n-1} + k$ behave as if the state at time 2^{n-1} were I_5^1 or I_5^4, and this decides the state of the leftmost two sites at time 2^n;

- all sites $(x, 2^{n-1}+k)$, $x \geq 2^{n-1}-k+1$ at time $2^{n-1}+k$ behave as if the state at time 2^{n-1} were the semi-infinite configuration $\ldots 11110011110011$, where the rightmost 1 is at $(2^{n-1}, 2^{n-1})$. As all blocks are even, one can use Lemmas 2.1, and 3.2 to get the claimed state of the remaining sites at time 2^n.

Finally, the last claim follows by a direct verification. □

Our next configuration with boundary, I_7, initially has occupied sites only on the nonpositive part of the x-axis, where the configuration is

$$\ldots 11110011110011\underline{1},$$

and its occupation counts are given by

$$\nu_n = |A_\infty \cap \{(x,y) : 1 \leq y \leq 2^n, -y+1 \leq x \leq y\}|.$$

Lemma 4.3. *Starting from I_7, at time 2^n the line $y = 2^n$ has the following configuration*

$$\begin{aligned} &\ldots 001111\underline{111100111100\ldots 0011110011} \quad (n \text{ even}) \\ &\ldots 111100\underline{001111001111\ldots 0011110011} \quad (n \text{ odd}) \end{aligned}$$

(Here, the entire interval $[-2^n+1, 2^n]$ is underlined, and all states to the right of the specified configurations are 0's.) Moreover, the EBD B_t seals the wedge at time 2^n+1.

Proof. This time, the reader may consult Figure 3. The proof is even easier that that of Lemma 4.2: since all blocks in I_7 are even, we can directly apply Lemma 2.1 and Lemma 3.2. □

Our final initializations I_8^1 and I_8^2 have 0's off the x-axis and on the x-axis are given by:

$$\begin{aligned} &\ldots 11110011110\underline{0}001111001111\ldots \quad (I_8^1), \\ &\ldots 00111100111\underline{1}111100111100\ldots \quad (I_8^2), \end{aligned}$$

respectively. One pair of corresponding occupation counts are

$$\begin{aligned} \gamma_n =& |A_\infty \cap \{(x,y) : 1 \leq y \leq 2^n, -y+1 \leq x \leq y\}|, \\ & \text{from } I_8^1 \text{ (resp. } I_8^2\text{) if } n \text{ is odd (resp. even).} \end{aligned}$$

Lemma 4.4. *Starting from I_8^1 (resp. I_8^2), if n is odd (resp. even), then at time 2^n the line $y = 2^n$ has configuration*

$$\begin{aligned} &\ldots 001111\underline{1111001111\ldots 1111001111}111100\ldots \quad (n \text{ odd}) \\ &\ldots 111100\underline{0011110011\ldots 1100111100}001111\ldots \quad (n \text{ even}) \end{aligned}$$

Again, the EBD B_t seals the wedge at time 2^n+1.

Proof. This case is illustrated by Figures 4 and 5, and follows directly from Lemmas 2.1, 3.4, and 3.6. □

The other pair of counts for our last initialization are

$$\sigma_n = |A_\infty \cap \{(x,y) : 1 \le y \le 2^n, -y+1 \le x \le y\}|,$$
$$\text{from } I_8^1 \text{ (resp. } I_8^2\text{) if } n \text{ is even (resp. odd).}$$

Lemma 4.5. *Starting from I_8^1 (resp. I_8^2), if n is even (resp. odd), then at time 2^n-2, the interval $[-2^n+3, 2^n-2] \times \{2^n-2\}$ consists entirely of 1's, and four additional 1's are adjoined at each end of that interval, for the total of 2^n+4 1's. Consequently, apart from its bottom two lines, the wedge is sealed by the EBD B_t at time 2^n-2.*

Proof. Again, Figures 4 and 5 can be used as visual aids, and the argument makes direct use of Lemmas 2.1, 3.3, and 3.5. □

As time goes on from 2^n-2, the dynamics B_t leaves a triangular hole resulting from the 1's referred to in Lemma 4.5, while the dynamics A_t starts filling this hole from the two ends with exactly the same boundary conditions as those in the definition of β_n. Those two wedge dynamics do not interact before an additional time 2^n+1; hence (as they are sealed at that time) each results in β_n occupied sites.

Figures 2–5 illustrate the above lemmas, and generation of each of the 4 regions that determines the corresponding population counts, i.e., the β-, ν-, γ-, and σ-region. For these examples we have chosen sizes $2^5 = 32$, and the initial configurations specified in the definitions are colored black. The divisions of these regions into smaller ones are also outlined, and the types of the smaller regions are indicated by the macroscopic icons placed to the right in the figures. The fifth type of region, the 2/3-region, is never subdivided. Note that only in the division of a γ-region do the smaller regions overlap. To make the filling mechanism clearer, sites occupied by the EBD are shown in a darker shade of gray. We should also remind the reader that our y-axis is oriented downward.

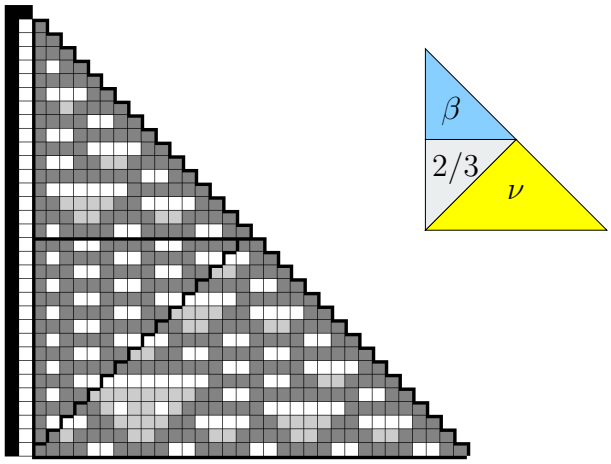

Fig. 2. Division of a β-region.

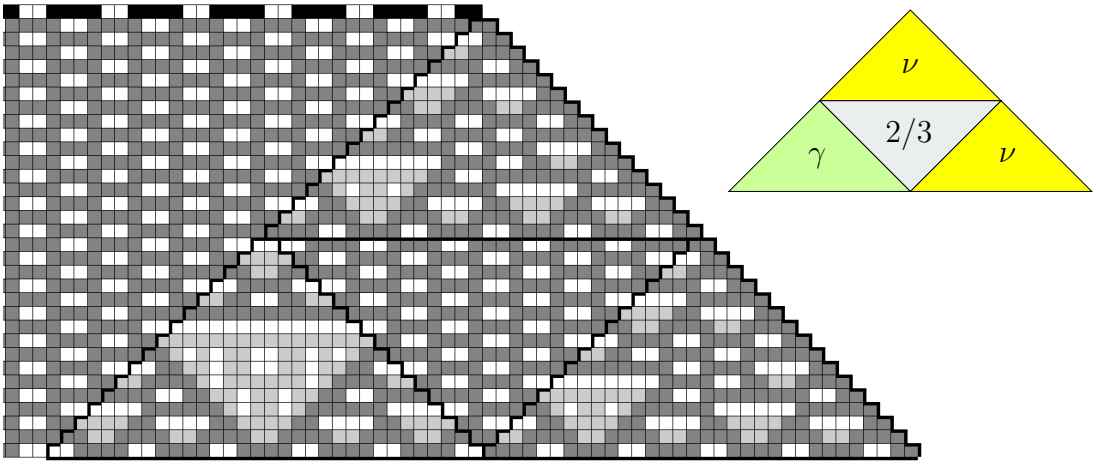

Fig. 3. Division of a ν-region.

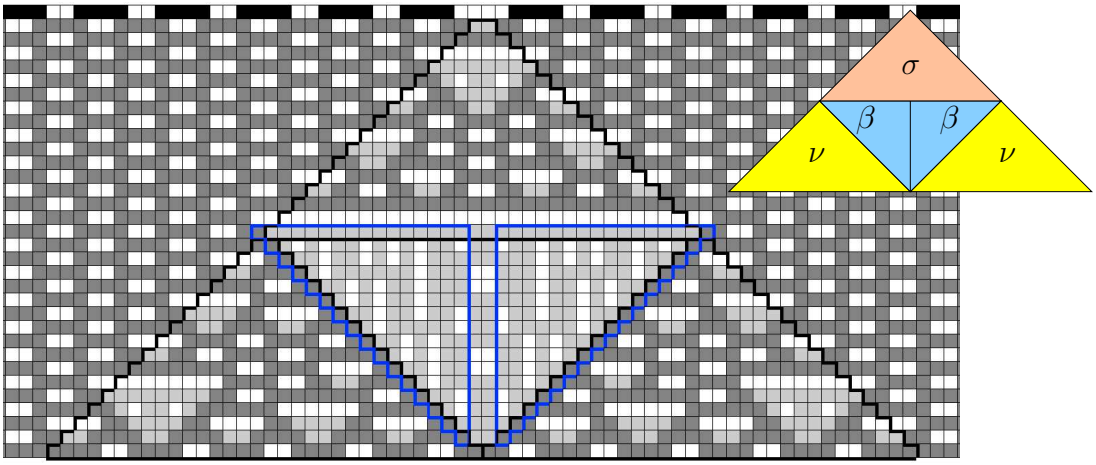

Fig. 4. Division of a γ-region.

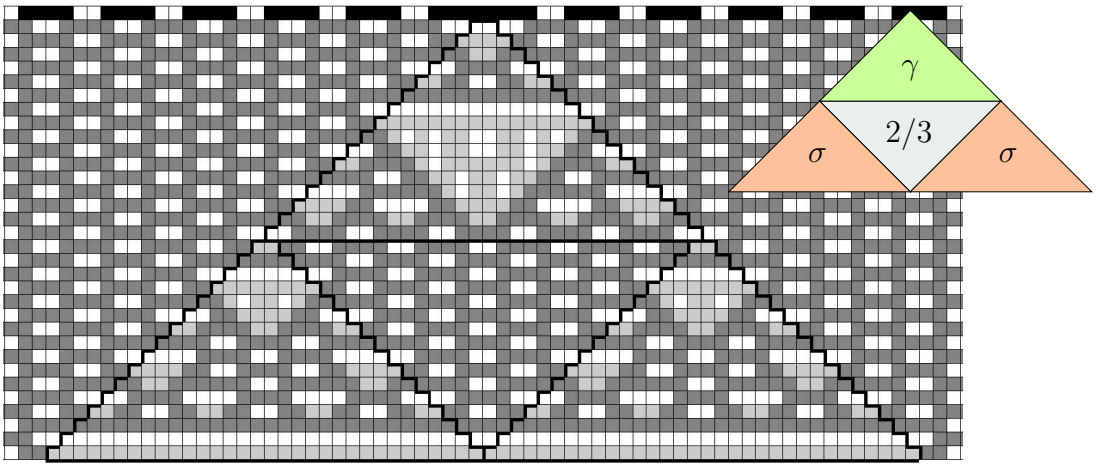

Fig. 5. Division of a σ-region.

The lemmas of this section, together with careful checking of boundary terms, result in the exact recursion

$$\begin{bmatrix}\beta_{n+1}\\ \nu_{n+1}\\ \gamma_{n+1}\\ \sigma_{n+1}\end{bmatrix} = A \begin{bmatrix}\beta_{n}\\ \nu_{n}\\ \gamma_{n}\\ \sigma_{n}\end{bmatrix} + 4^n\, y_4 + 2^n\, y_2 + (-2)^n\, y_{-2} + y_1 + (-1)^n\, y_{-1},$$

where

$$A = \begin{bmatrix}1 & 1 & 0 & 0\\ 0 & 2 & 1 & 0\\ 2 & 2 & 0 & 1\\ 0 & 0 & 1 & 2\end{bmatrix}$$

and

$$y_4 = \begin{bmatrix}1/3\\ 2/3\\ 0\\ 2/3\end{bmatrix}, \quad y_2 = \begin{bmatrix}-1/12\\ -2\\ 0\\ -2\end{bmatrix}, \quad y_{-2} = \begin{bmatrix}1/12\\ -4/3\\ -8/3\\ -4/3\end{bmatrix}, \quad y_1 = \begin{bmatrix}1/3\\ -4/3\\ 11/3\\ -7/3\end{bmatrix}, \quad y_{-1} = \begin{bmatrix}-2/3\\ -2\\ -1\\ -1\end{bmatrix}.$$

Let us briefly outline a derivation of the recursion for β_n, the first line of the above vector equation. The remaining lines can be derived similarly.

Write ω_n for the occupation count of the 2/3-region in Figure 2 (so that ω_4 is the count in that figure). For odd n, two such regions, joined at the diagonal, fit together to form a $(2^n-1)\times 2^n$ array. In this array, 0's are arranged into a pattern of dominoes: $(2^n-2)/3$ columns of 2^{n-1} dominoes each. Thus, for odd n, $\omega_n = 4^n/3 - 2^n/6$. For even n, two joined 2/3-regions produce a $(2^n+1)\times(2^n-2)$ array with two additional occupied cells. In the array,

there are $(2^n-4)/3 \times (2^{n-1}-1)$ dominoes, as well as 2^n-2 singletons, of 0's. Thus, for even n, $\omega_n = 4^n/3 - 1/3$. From the left, the final row of the ν-region starts $001111\ldots$ for odd n, and $111100\ldots$ for even n. Due to the solid left boundary of the β-region, an additional 1 is therefore contributed to β_{n+1} when n is odd. Hence the decomposition of Figure 2 yields

$$\beta_{n+1} = \beta_n + \nu_n + \omega_n + 1_{\{n \text{ odd}\}},$$

and the claimed recursion for β follows.

The matrix A has largest eigenvalue $\lambda_1 \approx 3.214$, the largest root of $\lambda^3 - 3\lambda^2 - \lambda + 1 = 0$, next largest eigenvalue 2, and two other eigenvalues $\lambda_2 \approx -0.675$ and $\lambda_3 \approx 0.461$. The next result is immediate.

Lemma 4.6.

$$\beta_n = \frac{1}{3} \cdot 4^n + r_1' \cdot \lambda_1^n + r_+ \cdot 2^n + r_- \cdot (-2)^n + \mathcal{O}(1),$$

for suitable constants r_1', r_+, r_-. The expansions for ν_n, γ_n, and σ_n have the same form.

Note that there is no resonance term $n\,2^n$ because y_2 is in the image of the singular matrix $A - 2I$. We also mention that the population counts are achieved already at time 2^n for β_n, ν_n and γ_n, while the σ_n–region fixates, apart from its bottom row, at time $2^n - 2$. This can be proved easily by induction.

Another fact that we will exploit in the next section is the following lemma, which is needed to handle general initial states. Namely, due to Lemma 2.4, off a bounded perturbation of the Sierpinski lattice, the available space $\mathbb{Z}^2$ can be subdivided into domains that each fill exactly like the β-region of an appropriate size. However, due to the perturbation, the dynamics on these domains may interact slightly too early, i.e., the time of the early onset of interaction is uniformly bounded. We thus need to demonstrate that this nuisance only mildly affects the occupation count.

Lemma 4.7. *For every integer $m \geq 0$ there exists another integer $M = M(m)$ so that the following is true. Assume that the dynamics, starting from I_6, is stopped at some time $2^n - m$. At this time, suppose the configuration outside the wedge $\{(x,y) : 1 \leq y \leq 2^n, 1 \leq x \leq y\}$ in the definition of β_n is arbitrarily changed. Such a change does not affect the truncated wedge count $|A_\infty \cap \{(x,y) : 1 \leq y \leq 2^n - M, 1 \leq x \leq y\}|$.*

Proof. Construct a *good* division of the original wedge into regions, as in the Figures 2–5, so that the only regions intersecting the outside of the truncated edge are ν-regions, and 2/3-regions oriented downward, in the sense that this is the direction in which the bricks are laid. Moreover, we require that the ν-regions that intersect the outside of the truncated wedge are smaller than $24m$ in diameter. All other regions seal before the outside has a chance to affect them (by a speed of light argument) and the intersections between the 2/3-regions and the truncated wedge are unaffected because of the remarks at the beginning of this section.

A formal way to see that a good division exists is as follows. Start with a large m, and with a large β-region, which is subdivided as in Figure 2. All further subdivided regions will

be ν-regions, and their subdivision is indicated in Figure 6. We keep track only of the regions that reach the bottom edge, as others are not relevant until the sizes become small. Note that for any rotated ν-regions as in Figure 6, one can further subdivide them using the division of Figure 3, since only a smaller ν-region is relevant.

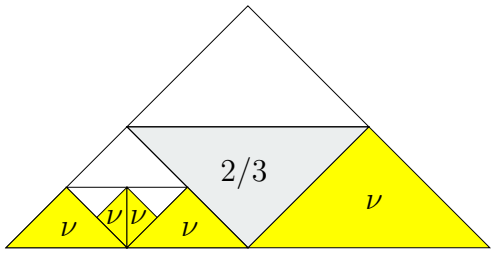

Fig. 6. Replacement of a ν-region by smaller regions that extend to the bottom edge.

Thus, a ν-region can be replaced by a 2/3-region, and five ν-regions, with a diameter reduction of 1/2 (one region), 1/4 (two regions), and 1/8 (two regions, rotated). A rotated ν-region can be replaced by a rotated ν-region of half the diameter. We continue to perform this replacement operation for any relevant ν-region, unless its diameter falls below $24m$. All the resulting relevant regions have their diameters at least $3m$ and hence, by construction, cover all points within distance $3m/2 > m$ of the bottom of the original wedge. □

5 The densities of *Box 12* and its cousins

We are now prepared to prove the first part of Theorem 1.

Proof. (*Theorem 1, Group 1.*) We first treat *Box 12*, then describe the needed modifications for other rules in Group 1. Assume the seed Λ is a subset of the x-axis, with its leftmost 1 at the origin and rightmost 1 at $(b, 0)$. We only need to consider such sets, as the argument will show that the density is completely determined by the EBD and hence by configurations on the four lines $\{x = m_1\}$, $\{x = M_1\}$, $\{y = m_2\}$, $\{y = M_2\}$, where m_i (resp. M_i) are the smallest (resp. largest) numbers for which the corresponding sets are nonempty.

Consider the final configuration within the wedge $W = \{(x, y) : y \geq 0, -y \leq x \leq y + b\}$, and introduce the count

$$\alpha_n = |A_\infty \cap W \cap \{y \leq 2^n\}|.$$

Also, consider the corresponding set Λ_0 from Lemma 2.4, translated so that its leftmost 1 is at the origin and rightmost 1 at $(b', 0)$, and define the count α'_n analogously. By Lemma 2.4 and Lemma 4.7,

$$\begin{aligned} \alpha_{n+1} &= \alpha_n + 2\alpha'_n + 2\beta_n + \mathcal{O}(2^n), \\ \alpha'_{n+1} &= 3\alpha'_n + 2\beta_n + \mathcal{O}(2^n). \end{aligned} \tag{4}$$

An iconic representation of the first line of (4) is Figure 7. It is important to observe that the two β-regions grow horizontally into the triangular void, that the last sentence of Lemma 2.4

provides the justification for using the boundary condition I_6, and that Lemma 4.7 guarantees that the interaction of the two can cause a perturbation of at most $\mathcal{O}(2^n)$.

From (4), by Lemma 4.6 and standard linear algebra,

$$\alpha_n = \rho \cdot 4^n + r_1 \cdot \lambda_1^n + r_2 \cdot 3^n + \mathcal{O}(2^n), \tag{5}$$

for suitable constants r_1 and r_2, where $\rho = 2/3$; α'_n has an expansion of the same form.

Take the box $[-1,1]^2 \subset \mathbb{R}^2$. Divide it into 4 triangles by the diagonals. Each of these triangles is called an α-region, as it is a macroscopic representation of a region in the definition of α_n. Such a region divides into an α-region, two α' -regions and two β-regions, as in the left icon of Figure 7, and corresponding to the first line of recursion (4). We call this the *first order* division of an α-region. Each of the resulting regions can be subdivided: an α-region in the same fashion, an α'-region very similarly into three α'-regions and two β-regions, and a β-region as in the icon on the right of Figure 2, giving rise to the *second* order subdivision (see the right icon of Figure 7, where types of regions are color-coded but not indicated by letters). This can be iterated, using Figure 7 and Figures 2–5, with the additional proviso that a (2/3)-region is subdivided into four congruent triangles at each step. We will use the notation D_k for a generic region that belongs to the k'th order subdivision (for example, D_2 could be any one of 21 second order regions). It is clear that the maximum diameter of a region D_k is 2^{-k+1}.

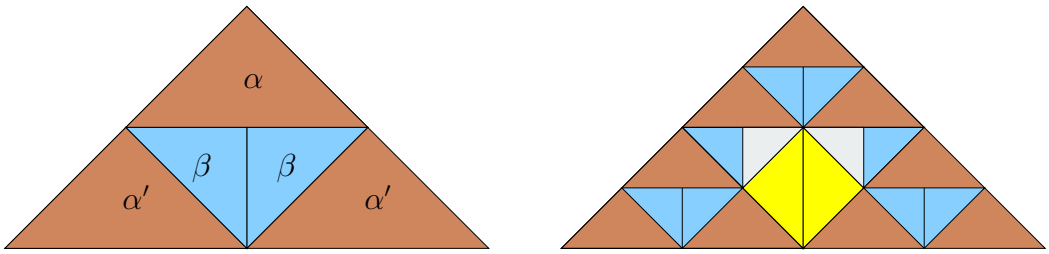

Fig. 7. First and second order division of an α-region.

Fix a square $R \subset \mathbb{R}^2$, and assume that it is included in the box $[-2^L, 2^L]^2$. Fix also a small $\delta > 0$, and a large integer k. For a given $\epsilon > 0$, let $n = L + \lceil \log_2(1/\epsilon) \rceil$ be the smallest n so that $\epsilon 2^n \geq 2^L$. The first step is to take ϵ so small (and thus n so large) that for every k'th order region D_k,

$$(\rho - \delta) \cdot \text{area}(2^n \cdot D_k) \leq |(2^n \cdot D_k) \cap A_\infty| \leq (\rho + \delta) \cdot \text{area}(2^n \cdot D_k).$$

That this is possible is trivial for 2/3-regions and otherwise follows from Lemma 4.6 and (5).

A lower bound on the number of sites in $R \cap (\epsilon \cdot A_\infty)$ is the combined number of sites which are in

$$(\epsilon 2^n \cdot D_k) \cap (\epsilon \cdot A_\infty)$$

for all regions D_k for which $\epsilon 2^n \cdot D_k \subset R$. Given the upper bound on the diameter of D_k, the combined area of these regions is at least

$$\text{area}(R) - 2 \cdot \text{perimeter}(R) \cdot \epsilon 2^n \cdot 2^{-k+1}.$$

Therefore

$$\epsilon^2 \cdot |R \cap (\epsilon \cdot A_\infty)| \geq (\rho - \delta) \cdot \text{area}(R) - 2 \cdot \text{perimeter}(R) \cdot 2^{L+1} \cdot 2^{-k+1}.$$

Send $\epsilon \to 0$, and then $\delta \to 0$ and $k \to \infty$, to conclude that

$$\liminf_{\epsilon \to 0} \epsilon^2 \cdot |R \cap (\epsilon \cdot A_\infty)| \geq \rho \cdot \text{area}(R).$$

The proof of the matching upper bound is analogous, proving Theorem 1 for the *Box 12* case. (A similar but somewhat harder argument appears in Section 6 of [**GG2**].)

Essentially the same reasoning goes through for all the Case I rules of Theorem 1. If $\{1, 2\} \subset S$, but $3 \notin S$, then the EBD stays the same, while $4 \notin S$ ensures that the modified EBD $\tilde{B}_t$ of Section 4 (with the same boundary conditions) is unchanged. The stated properties of $\tilde{B}_t$ in Lemma 4.1 continue to hold, while all sites (x, y) with $x \geq 3$ that are ever occupied by A_t are occupied by $\tilde{B}_t$. (On $x \leq 2$, A_t either solidifies completely or leaves a periodic pattern, but the 0's between bricks of 1's are sealed and thus unaffected.) Moreover, the inductive argument of Lemma 4.2 is unchanged, and so are Lemmas 4.3–4.5. For the eight Case I rules with $7 \notin S$, the 0's between bricks remain 0's, Lemmas 4.6 and 4.7 still hold, and the asymptotic density therefore remains 2/3. On the other hand, for the eight Case I rules with $\{1, 2, 7\} \subset S$, but $3 \notin S$ and $4 \notin S$, the 0's between the bricks change to 1's and the resulting density is 1.

The remaining Case I rules, with $\{1, 2, 4, 5\} \subset S$, but $3 \notin S$, need another minor change in the proofs of the previous section, which we now describe. The four initial states I_5^i are modified by deletion of the leading 0 so that the configurations begin with $\underline{1}$. Corresponding changes apply to Lemmas 4.1 and 4.2, so A_t and $\tilde{B}_t$ now occupy $(0, t)$ instead of $(1, t)$, and the shifted configurations are now achieved at time $2^n - 1$. (Observe that it is necessary that $5 \in S$ to *guarantee* occupation of $(0, t)$ by $\tilde{B}_t$, as $(0, t)$ sees at least 4 already occupied sites — three on the line $x = -1$ and one recursively at $(0, t-1)$ — and if $5 \notin S$ a 1 at $(1, t-1)$ may, and in fact will, interfere.) The remainder of the argument proceeds along the same lines as for *Box 12* and its variants of the preceding paragraph. Here the two 0's between adjacent bricks, at the time they are laid, see four 1's each, so the density is again 1. □

The proof of our theorem actually gives not only the dominant term in the population count expansion, but also the next two terms. It is interesting to note that these result from two fractal structures in the proof. The first fractal, featured in the previous section, results from appropriately scaled wedge dynamics (with the 2/3-regions of size more than 2, say, deleted) and has dimension $\log \lambda_1 / \log 2$. The second fractal is the familiar Sierpinski gasket generated by the scaled EBD in the proof just completed, which has dimension $\log 3 / \log 2$. See [**MW**, **Wil1**, **Wil2**] for more on fractal dimensions of such objects.

It takes considerable patience to determine by hand a closed formula for any featured population count. Instead, one could postulate the form of such a formula, with unknown constants, and proceed by curve-fitting. For *Box 12*, the form of the count $|A_\infty \cap B_\infty(0, 2^n - 1)|$ can be surmised from the recursion leading to Lemma 4.6. With a singleton at the origin as seed, we obtain the following remarkable formula for $n \geq 2$:

$$\frac{8}{3} \cdot 4^n + r_1 \lambda_1^n - \frac{8}{3} \cdot 3^n - \frac{16}{15} \cdot 2^n + \frac{2}{51} \cdot (-2)^n + 4n - 3 + \frac{8}{3} \cdot (-1)^n + r_9 \lambda_2^n + r_{10} \cdot \lambda_3^n,$$

where $\lambda_1, \lambda_2, \lambda_3$ were defined in the previous section, while

$$r_1 \approx 2.434\,,\ r_9 \approx -2.126\,,\ r_{10} \approx -6.614$$

solve $3145r^3 + 19832r^2 - 22688r - 107648 = 0$. A 2×2 box as seed yields a simpler formula, with no n, constant, or $(-1)^n$ term, and with the constant in front of 2^n changed to 18/5.

6 The densities of *Box 124* and its cousins

Let us now turn to the second part of Theorem 1, focusing on *Box 124*. We offer counterparts to the preliminary results of Section 4, beginning with the analogue of Lemma 4.2.

Lemma 6.1. *Starting from I_6, $\tilde{B}_t$ and A_t occupy at least $(t-1, t)$ and (t, t), for all $t \geq 0$. Moreover at time $2^n - 1$, $n \geq 1$, $\tilde{B}_t$ and A_t completely occupy the interval $[0, 2^n - 1] \times \{2^n - 1\}$.*

Proof. After a direct verification for $n = 1, 2$, one proceeds by induction. For the $n - 1 \to n$ step, note first that the induction hypothesis implies that $\tilde{B}_t$ occupies only a pair of sites at time 2^{n-1}, at $(2^{n-1} - 1, 2^{n-1})$ and $(2^{n-1}, 2^{n-1})$. By Lemma 2.1, speed of light, and properties of the linear dynamics, the entire interval $[1, 2^n - 1] \times \{2^n - 1\}$ is occupied. The site $(0, 2^n - 1)$ does feel the boundary condition at time $2^n - 1$ but it becomes occupied because, as the occupation spreads to the left from the pair at time 2^{n-1}, $(1, 2^n - 2)$ is occupied at the previous time, and $(0, 2^n - 1)$ sees that cell and three additional 1's on the line $x = -1$. See Figure 8, in which again dark grey are the sites occupied by $\tilde{B}_t$, for an illustration. □

Our next lemma deals with the case when the growth from I_6 is stopped by a horizontal line of 1's, and is needed because some β-regions defined below do grow with this constraint (e.g., the bottom β_4 region in Figure 8, which spreads *horizontally*).

Lemma 6.2. *Start now from I_6 together with additional occupied sites on the line $y = 2^n$. At time $2^n - 1$, the configuration of A_t within the interval $[0, 2^n - 1] \times \{2^n - 1\}$ is*

$$\underline{0}001100110011 \ldots 0011001.$$

Moreover, this configuration never changes afterwards.

Proof. Let us start at time 2^{n-1}. The previous lemma applies, and, as in its proof, $\tilde{B}_t$ occupies only two sites $(2^{n-1} - 1, 2^{n-1})$ and $(2^{n-1}, 2^{n-1})$ at this time. This configuration, by Lemma 2.1 and properties of the linear dynamics, generates

$$\underline{0}1100110011 \ldots 0011,$$

on $[0, 2^n - 2] \times \{2^n - 2\}$ at time $2^n - 2$ (when the boundary condition at $y = 2^n - 1$ is not yet felt). All that now remains is a direct verification. □

Next consider the initial state I_9, which has 1's only on the nonpositive part of the x-axis, and 0's elsewhere.

Lemma 6.3. *From I_9, at time 2^n the interval $[-2^n+1, 2^n] \times \{2^n\}$ consists entirely of 1's, under both A_t and B_t.*

Proof. At $t = 1$, B_t occupies only two sites, $(0, 1)$ and $(1, 1)$, and the claim once again follows from Lemma 2.1. □

Proof. (*Theorem 1, Group II.*) The last three lemmas make this case quite straightforward. Indeed, starting from I_6, we now redefine

$$\beta_n = |A_\infty \cap \{(x, y) : 0 \le y \le 2^n - 1, 0 \le x \le y\}|,$$

and starting from I_9,

$$\nu_n = |A_\infty \cap \{(x, y) : 1 \le y \le 2^n, -y + 1 \le x \le y\}|.$$

Then Lemma 6.2 determines the last layer of the β-region growing leftward, and after some easy counting we get

$$\begin{aligned} \beta_n &= 2\beta_{n-1} + \nu_{n-1} - 3 \cdot 2^{n-2} - 1, \\ \nu_n &= 2\beta_{n-1} + 3\nu_{n-1} - 2^n, \end{aligned} \tag{6}$$

valid for $n \ge 3$, with $\beta_2 = 9$, $\nu_2 = 20$. The reader may wish to consult Figure 8 for verification. (As the Group 2 rules are much simpler than those of Group 1, a single figure suffices.)

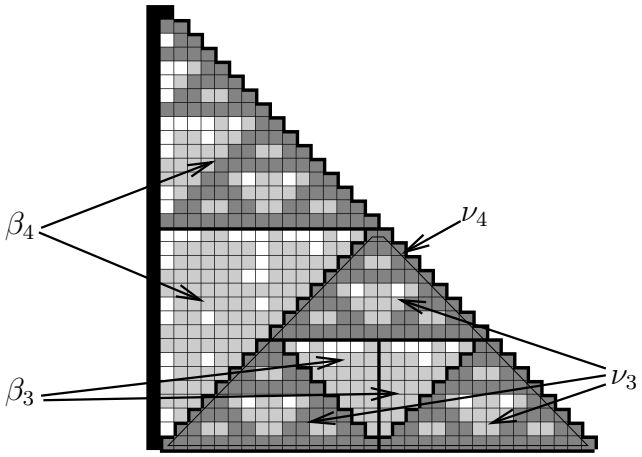

Fig. 8. Division of the β_5-region into two copies, one of which is approximate, of the β_4-region and one copy of the ν_4-region (outlined triangle). Also depicted is the division of the ν_4-region into three copies of the ν_3-region and two approximate copies of the β_3-region.

One can solve the recursion to get

$$\beta_n = \frac{65}{144} \cdot 4^n + \frac{1}{4} \cdot 2^n - \frac{2}{3} \cdot n + \frac{19}{9}.$$

In particular, with $\rho = 65/72$, $\beta_n = \frac{1}{2}\rho \cdot 4^n + \mathcal{O}(2^n)$ and then $\nu_n = \rho \cdot 4^n + \mathcal{O}(2^n)$. The rest of the proof for *Box 124* proceeds along the lines of the proof in Section 5. Other rules in this group are handled similarly, but note that for Group II the density is affected by inhomogeneous terms in recursion (6) and its initial conditions, which explains the many different densities. □

7 *Box 13*

As mentioned in the Introduction, the EBD for *Box 13* is additive, and given by $\bar{\ell}_t$, or its space-time variant $\bar{L}_t$. Consider a singleton at the origin as the seed. At time $t = 2^n - 1$ the state of $\bar{\ell}_t$ has all 1's confined to the interval $[-(2^n - 1), 2^n - 1]$, within which the state is

$$11011\ldots110\underline{1}011\ldots11011 \quad \text{or}$$
$$11011\ldots101\underline{1}101\ldots11011$$

depending on whether n is even or odd, followed at the next time by 1's only at $\pm 2^n$ and 0. While this dynamics has replication properties similar to ℓ_t, its state at time $2^n - 1$ is not solid and thus $\bar{L}_t$ does not seal the bottom edge of the triangle: 0's can change into 1's later and alter other sites within the triangle.

It is therefore natural to look at the *two-level* EBD $\bar{\ell}^2_t$ and $\bar{L}^2_t$, which track the two most extreme levels of A_t. Assume the state of $\bar{\ell}^2_t$ is included in $\mathbb{Z} \times \{-1, 0\}$. Given $\bar{\ell}^2_t$, initialize with $A_0 = \bar{\ell}^2_t$, apply the *Box 13* rule to compute A_1, take the bottom two rows and translate them back:

$$\bar{\ell}^2_{t+1} = A_1 \cap (\mathbb{Z} \times \{0, 1\}) + (0, -1).$$

The corresponding space-time rule $\bar{L}^2_t$ allows *Box 13* updating from time t to time $t+1$ to take place only on the lines $y = t$ and $y = t + 1$. (For comparison, the one-level EBD update of $\bar{L}_t$ takes place only on the line $y = t + 1$.)

Although it is no longer additive, the two-level EBD is much more useful for *Box 13*. The following lemma provides some immediate evidence by showing that $\bar{L}^2_t$ seals diagonal edges.

Lemma 7.1. *Assume that $\bar{L}^2_0 = A_0 \cap \{y \in \{-1, 0\}\}$ has its rightmost 1 on the line $y = 0$ at the origin, and that A_0 has no 1's on sites with y-coordinate strictly positive. Then sites on the lines $y = x$ and $y = x - 1$, $x \geq 2$, have the same state in A_∞ and in $\bar{L}^2_\infty$.*

Proof. The claim on the line $y = x$ is trivial since the EBD alone makes all those sites 1. We need to check that a 0 on the line $y = x - 1$, and in $\bar{L}^2_\infty$, cannot be changed to 1 by A_t. A 0 at $(t - 1, t)$ at time t and $t + 1$ implies the following configuration around it at time $t + 1$ (in both A_t and $\bar{L}^2_t$)

$$\begin{array}{ccc} 1 & 1 & \\ & 0 & 1 \\ & & 1 \quad 1 \end{array}$$

and so the 0 sees at least four 1's thereafter. □

We continue with some simple observations. Consider the configurations

$$J_1^1 = \begin{matrix} \ldots 011011011011 \ldots \\ \ldots 011011011011 \ldots \end{matrix}$$

$$J_1^2 = \begin{matrix} \ldots 1aa1aa1aa1aa \ldots \\ \ldots 011011011011 \ldots \end{matrix} \quad ,$$

where the states labeled a on the top line are such that each 1 on that line has at least one additional 1 next to it. For both J_1^1 and J_1^2, A_t will never change a state on the bottom line. Therefore no site above them can influence a site below.

Next, let us introduce some perturbations of these two kinds of "ether." More precisely, consider finite intervals two rows wide adjacent to segments of the J_1^i. A *left nucleus* is a finite interval in brackets, together with any overlined sites, in one of the following six configurations:

$$\begin{matrix} \ldots 00 \left[\begin{matrix} \ldots & bb \\ \ldots & 0\mathbf{0} \end{matrix} \right] 11011 \ldots \\ \ldots 00 \left[\begin{matrix} \ldots & bb \\ \ldots & 0\mathbf{0} \end{matrix} \right] 11011 \ldots \end{matrix} \qquad \begin{matrix} \ldots 00 \left[\begin{matrix} \ldots & 1 \\ \ldots & 01 \end{matrix} \right] 01101 \ldots \\ \ldots 00 \left[\begin{matrix} \ldots & 1 \\ \ldots & 01 \end{matrix} \right] \mathbf{0}1101 \ldots \end{matrix}$$

$$\begin{matrix} \ldots 00 \left[\begin{matrix} \ldots & \\ \ldots & 11 \end{matrix} \right] 10110 \ldots \\ \ldots 00 \left[\begin{matrix} \ldots & \\ \ldots & 11 \end{matrix} \right] 10110 \ldots \end{matrix} \qquad \begin{matrix} \ldots 00 \left[\begin{matrix} \ldots & cc \\ \ldots & 0\mathbf{0} \end{matrix} \right] \overline{c}a1aa \ldots \\ \ldots 00 \left[\begin{matrix} \ldots & cc \\ \ldots & 0\mathbf{0} \end{matrix} \right] 11011 \ldots \end{matrix}$$

$$\begin{matrix} \ldots 00 \left[\begin{matrix} \ldots & d \\ \ldots & 01 \end{matrix} \right] \overline{1d}a1a \ldots \\ \ldots 00 \left[\begin{matrix} \ldots & d \\ \ldots & 01 \end{matrix} \right] \mathbf{0}1101 \ldots \end{matrix} \qquad \begin{matrix} \ldots 00 \left[\begin{matrix} \ldots & \\ \ldots & 11 \end{matrix} \right] a1aa1 \ldots \\ \ldots 00 \left[\begin{matrix} \ldots & \\ \ldots & 11 \end{matrix} \right] 10110 \ldots \end{matrix}$$

Here the a's are as before, while the b's, c's and d's are chosen so the bold $\mathbf{0}$'s do *not* see one or three 1's. Other sites in the bracketed intervals have arbitrary state. A *right nucleus* is a mirror image of a left one, and a *middle nucleus* is either flanked on both sides by segments of J_1^1 or on both sides by segments of J_1^2 and satisfies one of the three respective conditions on both sides. We mark the *position* of a left nucleus as (leftmost 1 on its bottom line)-1, and as the bottom left corner of the nucleus in the other two cases.

Assume the seed consists of a left, a middle, and a right nucleus, with the middle one positioned at the origin. Call such a state a *replicator* if there exists an m so that at space-time points $(x\,2^m, s\,2^m)$, $x \in \mathbb{Z}$, $s \geq 0$, the positions of the nuclei are precisely given by those (x, s) at which $\bar{\ell}_s(x) = 1$. Here $\bar{\ell}_0$ has 1's at 0 and ± 1. Furthermore, the nuclei are of one of six configurations described in the next paragraph, but we emphasize immediately that the ether is assumed to be one of the two prescribed types and does not change from the beginning. See [**Eva**] for an earlier instance of replicators in nonlinear CA, and [**Epp**] for many more examples.

The left nuclei are of type *EL* or *IL*, where *EL* occurs only at the extreme left of the system, while *IL* occurs everywhere else. Similarly, the right nuclei are of type *ER* or *IR*. The middle nuclei are of type *M3* or *M1*, where the first kind occurs by interaction of three nuclei, and the second is a successor of a single nucleus.

To verify the replicator condition, we need to check two properties:

- Each nucleus creates potential nuclei at the next rescaled time and space locations according to the following scheme: *EL*→ *EL, M, IR; ER*→ *IL, M, IR; IL, IR, M1, M3*→ *IL, M, IR*. Here, M is either *M1* or *M3*, to be determined by interactions.
- Potential nuclei landing at the same space location interact as follows. Two of any type annihilate. Three result in *M3*. A single M converts to *M1*, and in other cases remains of the same type as the potential nucleus.

It is already clear that the replicator condition is a finite condition to check, since one can catalog all possible interactions. Even easier to verify is the following criterion.

Lemma 7.2. *Assume first that M3 and M1 nuclei create the same configuration (up to translation) two rescaled time units later. Assume also that the replicator condition is satisfied up to rescaled time $s = 4$. Then it is satisfied at all times.*

If the first assumption is not satisfied, then replication at time $s = 6$ is required to ensure replication at all times.

Proof. It is easy to prove by induction that the only interactions not occurring from time 0 to time 1 are collisions between an *IL* and an *IR*. Furthermore, at time 3 isolated *EL*, *ER*, and *M1* (equivalent to *M3* by the first assumption) appear for the first time, creating the required three nuclei the next time. (By the same induction, isolated *IL* and *IR* never appear). The second, more general, case is checked similarly. □

Lemma 7.3. *The EBD applied to the seed at any time $2^m s$ results in a number of copies of identical (one-dimensional) configurations J_2 that begin and end with 1's and are separated by 0's. Moreover, the copies of J_2 have their left endpoints at nucleus positions.*

Proof. The positions are an easy verification, while the fact that they are identical follows from additivity of the EBD. □

Note that J_2 is actually an equivalence class (modulo translation) of configurations. We call a replicator *type 1* if J_2 is a single 1 or a configuration like this: $10 * \cdots * 01$ (with arbitrary states in place of the $*$'s); *type 2* if J_2 is of the form: $11 * \cdots * 11$; and *mixed type* otherwise. Finally, we extend the term *replicator* to any seed for $\bar{\ell}_t^1$ that eventually results in a replicator, and give it the same type.

To any seed A_0 for A_t, there are four corresponding seeds for the two-level EBD. The first is obtained by translating A_0 vertically until its 1's with the largest y-coordinate are on the x-axis, then taking the intersection with $\{y \in \{-1, 0\}\}$ as $\bar{\ell}_0^2$. The other three are obtained by applying the same operation to the rotations of A_0 by $\pi/2$, π and $3\pi/2$. Call A_0 a type 1 or type 2 replicator if all four one-dimensional seeds are replicators of the same corresponding type.

Theorem 2. *If A_0 is a type 1 replicator, then A_∞ has density $28/45$. A type 2 replicator results in density $1/2$.*

We remark that, under a proper normalization, a replicator of mixed type will generate a non-constant density. We will not discuss such cases.

Proof. We will only sketch the proof of Theorem 2. No new ideas are necessary, but establishing the basic recursion (7) apparently requires a somewhat tedious induction argument along the lines of pp. 263–265 in [**GG1**] for *Box 1* from $A_0 = \{0\}$. The last step, which establishes the convergence to a multiple of a Lebesgue measure, is similar to the proof in Section 5.

Let us begin by explaining the difference between the two cases. If A_0 is a replicator of either type, then any of its four two-level EBD's eventually encounters a state such as the ones depicted by the black sites in the two parts of Figure 9. The periodic configuration in the first column will forever remain unchanged and contributes exactly two occupied neighbors to every site to its right. Hence it functions as a boundary condition for A_t spreading downward in the depicted wedge. This dynamics has it own two-level EBD. (We often call this evolution *secondary*, but will avoid the term here). The nucleus for this two-level EBD is in the top of the second column: it consists of either a 0 and a 1 (Figure 9, left) or two 1's (Figure 9, right). In the first case, the two-level EBD (dark gray sites) creates holes that are filled in very much the same way as independent copies of the wedge. In the second case, however, the two-level EBD does most of the work itself and $A_\infty \setminus \bar{L}^2_\infty$ contributes only to boundary corrections.

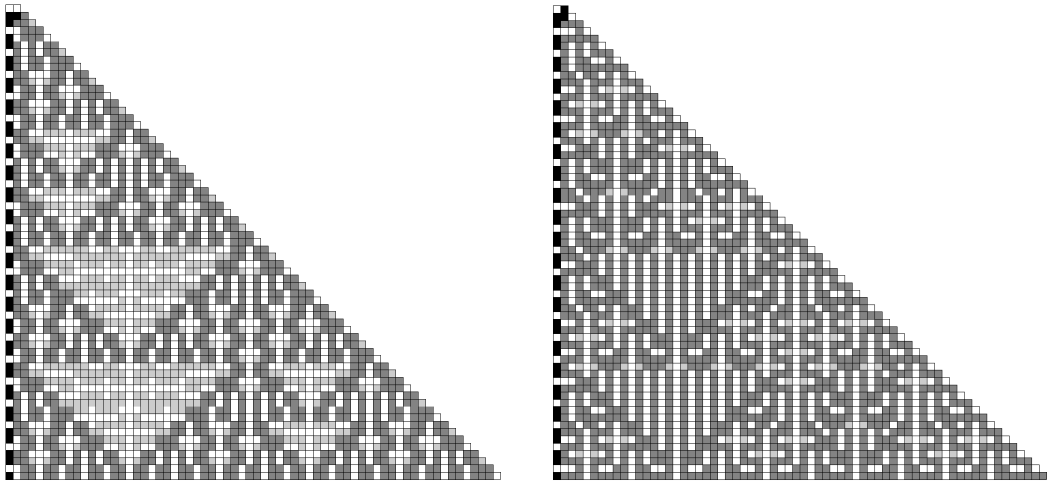

Fig. 9. Wedge dynamics for type 1 (left) and type 2 replicators. Sites occupied by the two-level EBD are darker.

Now consider the wedge population count for a type 1 replicator. Assume the nucleus is positioned so the black 1 in the second column in Figure 9 is at the origin, with boundary conditions also as in the figure. Redefine

$$\beta_n = |A_\infty \cap \{(x, y) : 0 \le y \le 2^n - 1, 0 \le x \le y\}|.$$

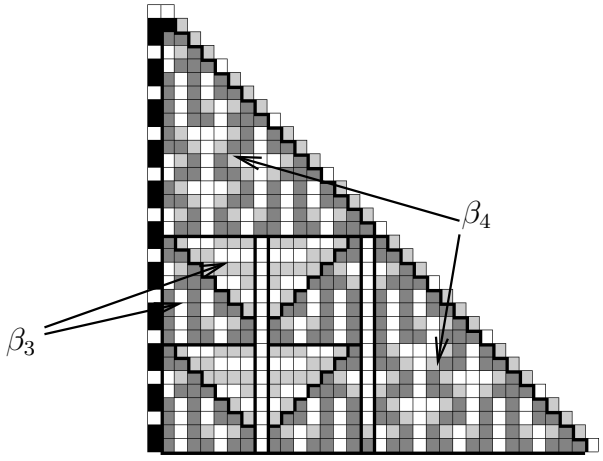

Fig. 10. Division of the β_5-region (for a type 1 replicator) into two copies of the β_4-region and eight approximate copies of the β_3-region (two of which are indicated by arrows). Here, only sites occupied by the EBD are dark gray.

After some counting (see Figure 10), we get $\beta_2 = 11$, $\beta_3 = 29$, and for $n \geq 4$

$$\beta_n = 2\,\beta_{n-1} + 8\,\beta_{n-2} - \frac{3}{2}\,2^n - 28 + (-1)^n. \tag{7}$$

The solution is, again for $n \geq 4$,

$$\beta_n = \frac{14}{45}\,4^n + \frac{3}{4}\,2^n + \frac{1}{36}\,(-2)^n + \frac{28}{9} - \frac{1}{5}\,(-1)^n.$$

This establishes the density for type 1 replicators.

For type 2 replicators, matters are simpler, as one does not need the exact count. Instead, we define β_n exactly as above, and note that

$$\beta_n = 2\beta_{n-1} + 4\beta_{n-2} + \frac{1}{16}\,4^n + \mathcal{O}(2^n).$$

From this it easily follows that

$$\beta_n = \frac{1}{4}\,4^n + r_1(1+\sqrt{5})^n + \mathcal{O}(2^n),$$

for an appropriate constant r_1. This formula gives density 1/2.

The remainder of the argument is similar to the proof of Theorem 1. □

It is easy to check that a singleton is a type 1 replicator, with J_2 consisting of a single point as well. In fact, for $n \geq 3$, $|A_\infty \cap [-(2^n-1), 2^n-1]^2|$ is given by

$$\frac{112}{45}\,4^n - 2\cdot 2^n + \frac{2}{9}\,(-2)^n + \frac{8(\sqrt{5}-2)}{5}\,(1+\sqrt{5})^n - \frac{8(\sqrt{5}+2)}{5}\,(1-\sqrt{5})^n + \frac{32}{5}\,(-1)^n + \frac{13}{45}\,.$$

An example of a type 2 replicator is

```
  1 1
1     1
1     1
  1 1
```

for which J_2 is the doublet 11. This is proved by Lemma 7.2 and Figure 11. Figure 12 provides a snapshot of the dynamics from the two seeds; Figure 13 shows two more examples of replicators.

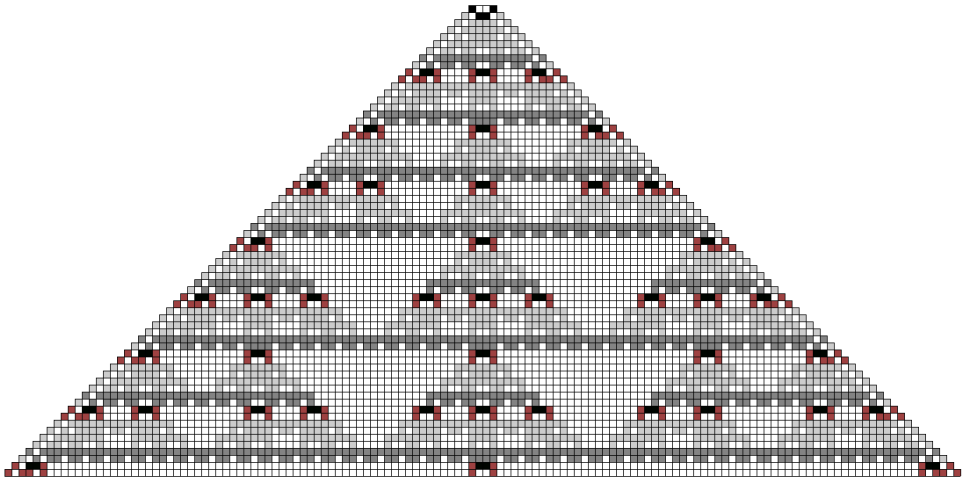

Fig. 11. The two-level EBD from the seed indicated in black in the first two rows. A type 2 replicator emerges already at time 4, but we have chosen the much more evident state at time 7 as the initial replicator. Henceforth the two-level EBD is depicted in dark gray at times $7+8s$, and in darker gray (with copies of J_1 in black) at times $7+8s+2$. (For illustration, the computation is carried up to $s = 7$ although the conditions of Lemma 4.2 are satisfied at $s = 4$.)

Are the two densities in Theorem 2 the only computable ones? The answer is no, and we will now mention several additional options. We suspect there are infinitely many possible rational densities. In these examples, we provide only a quarter of the seed for A_t, the one that governs the downward two-level EBD. It is easy to construct a full seed by creating a "frame" from four copies of this configuration (appropriately rotated and positioned), so that all four two-level EBD's are the same. Configuration

```
0111010
1010011
```

results in density 5/8, while

```
100111101110
111001111101
```

generates density 21/32. The last configuration flipped upside down yields the largest density we have found: 3/4.

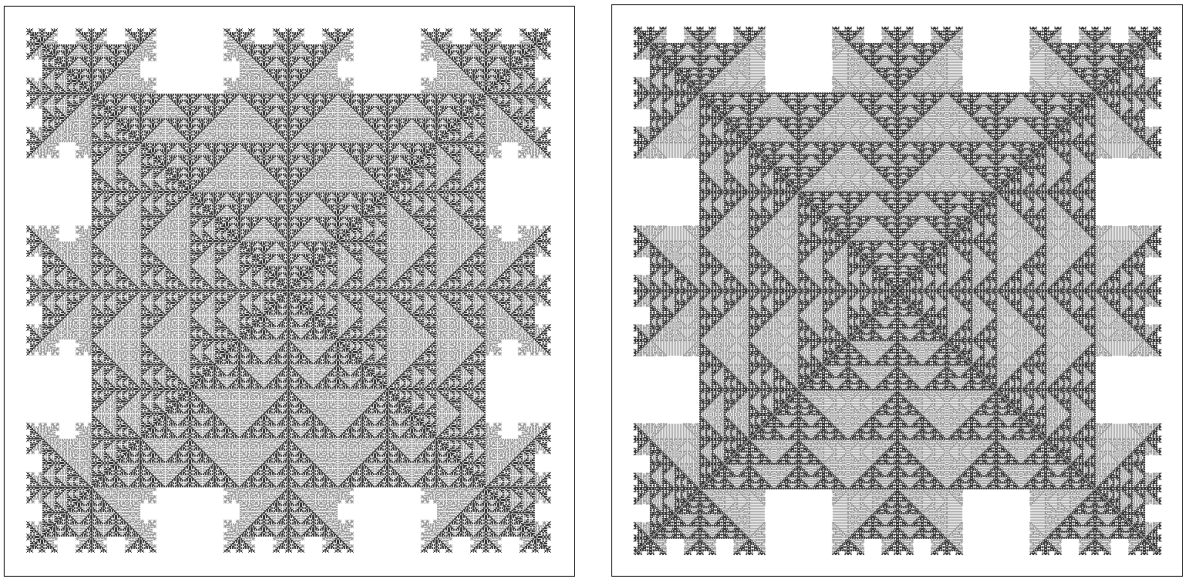

Fig. 12. Left: *Box 13* from a singleton, with density 28/45. Right: *Box 13* from a seed with density 1/2. Both are captured at time 340, and the two-level EBD is highlighted in both frames.

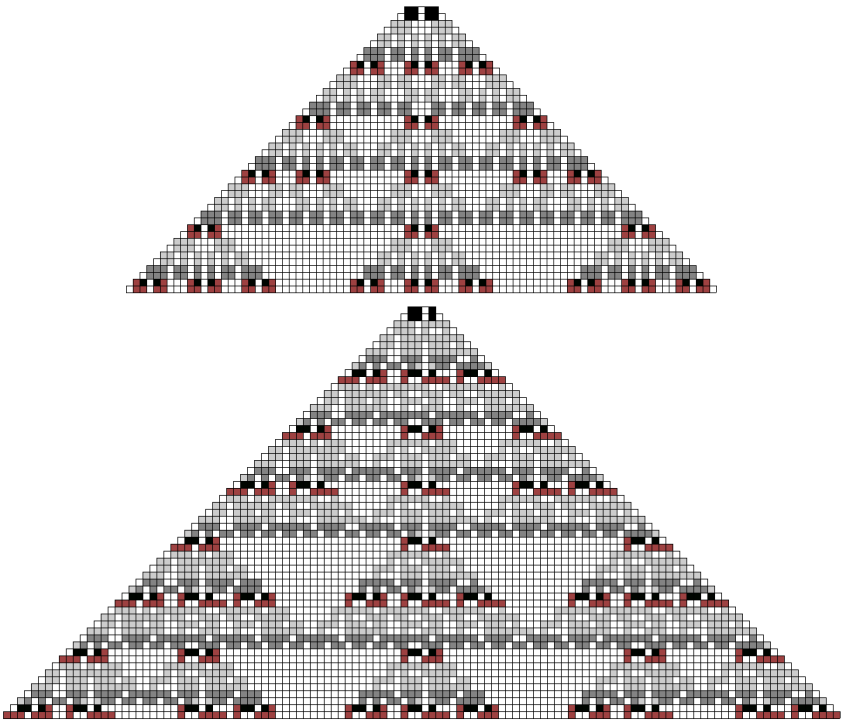

Fig. 13. More examples: a type 1 replicator, and one of mixed type, at times when the conditions of Lemma 7.2 are satisfied.

These densities can presumably all be rigorously established by induction arguments similar to, but much more involved than, the one sketched in this section. For instance, Figure 13 makes it clear that some replicator scheme for the two-level EBD exists, and then the resulting holes are filled by a periodic pattern that self-organizes after a constant time.

How common are replicators? This is an intriguing question to which we have no rigorous answer. By choosing seeds ℓ_0^2 that are random subsets of the $N \times 2$ box (with all 2^{2N} configurations equally likely), a replicator appears to emerge with substantial probability (at least bounded away from 0, if not actually approaching 1) for large N. Small seeds can be checked by hand. E.g., there are 29 subsets of the 3×2 box up to symmetry, which can be categorized as follows:

- nine type 1 replicators: 1 , $\begin{matrix}01\\10\end{matrix}$, $\begin{matrix}001\\100\end{matrix}$, $\begin{matrix}011\\100\end{matrix}$, $\begin{matrix}101\\010\end{matrix}$, 101 , $\begin{matrix}010\\101\end{matrix}$, $\begin{matrix}101\\111\end{matrix}$, $\begin{matrix}111\\111\end{matrix}$;
- seven type 2 replicators: 11 , $\begin{matrix}10\\11\end{matrix}$, $\begin{matrix}001\\110\end{matrix}$, $\begin{matrix}11\\11\end{matrix}$, $\begin{matrix}101\\110\end{matrix}$, $\begin{matrix}011\\110\end{matrix}$, $\begin{matrix}111\\110\end{matrix}$;
- and thirteen other cases that are apparently not replicators.

Of the seeds in the last category, two generate predictable behavior with provable density 1/2, namely $\begin{matrix}101\\101\end{matrix}$ and $\begin{matrix}111\\101\end{matrix}$. The other eleven seem to have very unpredictable behavior, which cannot however be adequately described as chaotic. Considerable multiscale structure (see Figure 14) would make *complex* a more fitting description. We refer the reader to [**NN**] for a recent text on complexity.

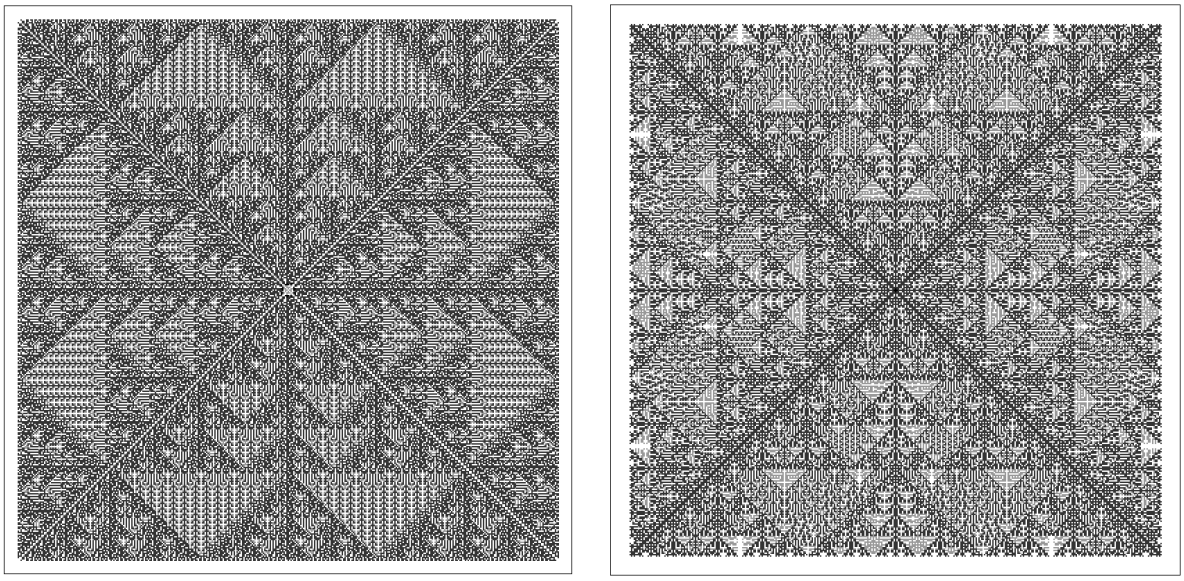

Fig. 14. Left: the example with density 5/8, at time 190. Note how the periodic region with

asymptotic density emerges quite late. Right: *Box 13* from the full von Neumann neighborhood, at the same time. Again, the two-level EBD is highlighted.

For comparison, we mention two rules that are apparently capable of truly chaotic growth. The first is *Box 1357* from a singleton (see [**Gri**] or [**Gra**] for snapshots of its evolution). However, one can check that the same rule fills the entire lattice starting from the full von Neumann neighborhood. Such examples help explain why we have restricted attention to *Box 13* in this section: adding any counts $i \geq 4$ to the solidification list introduces additional complications that are in most cases unmanageable. The second chaotic example is *Box 1* from an 8×8 box (see Figure 1 in [**Gra**]). (We have already noted that from a singleton, *Box 1* generates a replicator and density 4/9.) In this instance, $2 \notin S$ and $3 \notin S$, so the complications arise because the EBD lacks an additive component. A few additional results for these challenging remaining cases are the subject of our next and final section.

8 Remaining cases

The 32 Packard snowflakes with $2 \notin S$ and $3 \notin S$ have nonadditive EBD such that $b_t(x) = 1$ iff there is a single 1 in the set $\{b_{t-1}(x-1), b_{t-1}(x), b_{t-1}(x+1)\}$. From general seeds these boundary dynamics (also known as Rule 22 in the CA literature) are apparently chaotic. From certain seeds such as a singleton, however, a replicator emerges. Simulations on pp. 251, 262–3 of [**Wol2**] nicely illustrate the behavior.

As in the previous section, then, there is no prospect for recursive calculation of a common density from arbitrary seeds. Even if a replicator emerges, our technique only succeeds when all subsequent dynamics within the web's triangular holes are orderly. We have investigated the cases under discussion starting with only the origin occupied; the Sierpinski-type web for all these examples is shown in the upper-left figure on p. 263 of [**Wol2**]. As listed in Table 2, nontrivial asymptotic densities and exact counts are computable for 12 of the 32 rules. These results can all be proved using techniques from [**GG1**, **GG2**, **BDR**]; we omit the details.

rule	density	no. of sites	time	valid.
1, 18	4/9	$(16/9)\,4^n + (8/3)\,n - 7/9$	$2^n - 1$	$n \geq 1$
17, 178	35/72	$(35/18)\,4^n - 2 \cdot 2^n + (8/3)\,n + 41/9$	$2^n - 1$	$n \geq 2$
16	385/576	$(385/144)\,4^n - (3/2)\,2^n + (8/3)\,n + 89/9$	$2^n + 8$	$n \geq 4$
168	391/576	$(391/144)\,4^n - (5/2)\,2^n + (8/3)\,n + 137/9$	$2^n + 8$	$n \geq 4$
167, 1678	409/576	$(409/144)\,4^n + (8/3)\,n - 223/9$	$2^n + 8$	$n \geq 4$
15	43/72	$(43/18)\,4^n - (8/3)\,n + 217/9$	$2^n + 8$	$n \geq 3$
158	65/96	$(65/24)\,4^n - 4 \cdot 2^n - 8 \cdot n + 179/3$	$2^n + 8$	$n \geq 3$
156	8/9	$(32/9)\,4^n - (15/4)\,2^n + (160/3)\,n - 1823/9$	$2^{n+1} + 13$	$n \geq 5$
1568	2099/2304	$(2099/576)\,4^n - 4 \cdot 2^n + (160/3)\,n - 1775/9$	$2^{n+1} + 14$	$n \geq 5$

Table 2. Population counts starting from a singleton at the origin, on $[-(2^n - 1), 2^n - 1]^2$, at the fixation time.

We note that in three cases the dynamics are identical whether or not $8 \in S$. One can also

check that *Box 138* evolves exactly like *Box 13* from a singleton. In each of these cases, the *Box* rule with $8 \notin S$ never creates a 0 completely surrounded by 1's. In general, the final crystal A_∞ for a rule with $8 \in S$ is obtained by filling all the isolated holes in the final crystal for the corresponding rule with $8 \notin S$. See [**BDR**] for further discussion in the *Diamond* setting.

For some Packard rules that do not have an additive component, it can be proved by special arguments that they occupy almost all sites. We offer two notable examples below, but keep in mind that various degrees of filling the plane are in general possible. For instance, among the *Box* rules covered by Theorem 1, started from a singleton, *12567* fills Z^2 completely, *12467* fills off a finite set, *12457* fills off a dyadic set along the axes, and *1267* fills off a (discrete) fractal. Even *Box 123* in general fails to fill a neighborhood of the diagonals. We will not attempt to formulate a general result; see Theorem 3 in [**GG2**] for more on this and other microscopic properties of the *Hex* rules.

Theorem 3. *Box 145678 generates density 1 from any seed. In fact,* $|A_\infty^c \cap [-2^n, 2^n]^2| = \mathcal{O}(2^n)$.

Proof. We will prove that A_∞ covers all sites at more than a bounded distance from the axes and diagonals $y = \pm x$. For this, let us first consider the final set F_1 generated by the downward EBD B_t. We assume that the rightmost of the 1's in A_0 with largest y-coordinate is at 0. Note again that, for $t \geq 1$, B_t then occupies (x, t) at time t iff there is exactly one occupied site among $(x-1, t-1)$, $(x, t-1)$, and $(x+1, t-1)$.

We will show that *Box 45678*, started from F_1, generates a final set F_2 that covers all of the set $\{0 \leq x \leq y\}$ except for points a bounded distance away from its boundary. Since the critical threshold growth CA *Box 45678* is monotone [**GG1**, **Gra**], this will establish the requisite solidification on an eighth of the lattice, and by symmetry this is enough.

As remarked above, the EBD is not additive, so F_1 is in general not easy to describe completely. However, we can use the fact that, for each $m \geq 1$, the dynamics on the rightmost $m+1$ sites is closed (i.e., independent of what occurs elsewhere). We denote these dynamics by $\eta_t^m \in \{0,1\}^{[-m,0]}$, so that, by definition, $\eta_t^m(x) = 1$ iff B_t occupies $(t+x, t)$. Therefore, the process η_t^m always has $\eta_t^m(0) = 1$, and its state space has 2^m elements. As η_{t+1}^m only depends on η_t^m , it must eventually enter a cycle. Next are the two key observations.

> *Fact 1*: For $m = 2$, the only cycle is $111 - 001$, while the other two states are transient.
>
> *Fact 2*: Successive configurations of the limit cycle do not have two 0's in a row at the same positions.

Fact 1 is easy to check. To prove *Fact 2*, suppose that $[-i, -i+1]$, $i \geq 2$, is the position of rightmost pair of 0's in a cycle. We may assume that $m = i$, and then, for infinitely many times t, η_t^m has 001 at its left end, while η_{t+1}^m begins with 00. But the rule then dictates that η_{t+1}^m begins with 1, a contradiction.

Using *Fact 1*, let N be such that η_t^3 is in state 111 at $t = N$ and periodic thereafter. We claim that, for each $m \geq 2$, F_2 contains the "fattened diagonal"

$$D_m = \{(i,j) : j \geq N, i \geq N-2, i \leq j \leq i+m\}.$$

We prove the claim by induction. For $m = 2$, this follows easily from *Fact 1*. The $m - 1 \to m$ step is also a straightforward verification using *Fact 2*.

It follows that F_2 contains $\cup_{m\geq 2} D_m$, which completes the proof. □

There are rare initial sets such that $|A_\infty^c \cap [-2^n, 2^n]^2|$ is of order 2^n. The example of smallest cardinality we know has 32 sites and is shown in Figure 15.

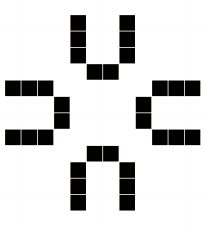

Fig. 15. An initial set for *Box 145678* that leaves the diagonals empty.

It is an intriguing open question whether Theorem 3 holds for *Box 15678*. We have no evidence against this claim; however, unlike *Box 145678*, this rule is capable of leaving a *finite* hole and thus the lessons of *Hex 1456* [**GG1**] suggest the possibility of an asymptotic density less than 1.

Theorem 4. *Any Box rule with* $\{1, 3, 4, 5\} \subset S$ *generates density 1 from any seed, and* $|A_\infty^c \cap [-2^n, 2^n]^2| = \mathcal{O}((1 + \sqrt{5})^n)$.

Proof. Later in the argument we will need to make use of the *three-level EBD* $\bar{\ell}_t^3$ tracking the three extreme levels of A_t. To begin, though, consider the two-level version $\bar{\ell}_t^2$. As already mentioned, cases with $2 \in S$ are easy, so we will skip them. Otherwise, the rules of the theorem all have the same two-level EBD. Pick two 1's on the first (bottom) level. Call them *connected* if they are connected in the neighborhood graph within the two levels. This notion divides first-level 1's into k *components*, each marked by the position of its leftmost and rightmost 1. Assume $a \leq b$ mark a component at time t, and let $a_1 \leq b_1$, $a_2 \leq b_2$ mark the components to its left and right (allow for $a_2 = \infty$ or $b_1 = -\infty$ if one or both fail to exist).

Then, the two-level EBD occupies all sites $(-1, i)$, $a \leq i \leq b$ at the next time, as is easy to check. Moreover, if $b \leq a_2 - 3$ and $a \geq b_1 + 3$, the component extends by one in each direction and is at time $t + 1$ marked by $a - 1$ and $b + 1$. Otherwise we say that a *collision* occurs at time t. We call this collision *coalescing* if $b = a_2 - 1$, or if $b = a_2 - 2$ and the 0 at position $b + 1$ on the first level generates a 1 on the second level at time $t + 1$. Otherwise we call the collision *annihilating*. Analogous conditions are imposed at the left end. A coalescing collision connects the components at time $t + 1$, whereas an annihilating collision does not.

It is easy to check that any collision scenario can only decrease the number of components from time t to time $t+1$. Therefore, the number is eventually constant, which we assume is true from time $t = 0$. In particular, this implies that any annihilating collision at time t_0 produces a 0 at time $t_0 + 1$ which, at this time and within the two levels, is connected on both sides to 1's

on the first level, like the 0 on the second (top) level in this example:

$$\begin{array}{cccccccccccc} & 1 & 1 & 1 & 1 & 1 & 0 & 1 & 1 & 1 & 1 & \\ 1 & 0 & 0 & 0 & 0 & 0 & \underline{0} & 0 & 0 & 0 & 0 & 1 \end{array} \tag{8}$$

This is true because in a configuration such as

$$\begin{array}{ccccc} 0 & 1 & 1 & 0 & 1 \\ \underline{0} & 0 & 0 & 0 & \end{array}$$

the component between the two 0's on the second level suffered annihilating collisions at both ends and got eliminated completely, precluding the possibility of a constant number of components.

How does a configuration such as (8) evolve? The two first-level 1's approach each other at light speed. Assume, as is customary, that the $\underline{0}$ is at the origin, and label positions on the x-axis of the two first level 1's at the time t_0+1 by b_0 and a_0. Further, assume that $b_0 \le -4$ and $a_0 \ge 4$. Then, at time t_0+4, sites on the *third* level of the three-level EBD ℓ_t^3 solidify between the first level 1's. To be more precise, all the following sites are 1 at times t_0+k, for $k \ge 4$: $(i,-3)$, $b_0+k \le i \le a_0-k$, $4 \le k \le (a_0-b_0)/2$.

For example, from time t_0+2 on, our example (8) has three-level EDB (where "?" denotes a site whose state cannot be surmised from the given states):

$$\begin{array}{cccccccccc} & 1 & 1 & 1 & 1 & ? & 1 & 1 & 1 & \\ & 1 & 1 & 1 & 0 & 0 & 0 & 1 & 1 & \\ 1 & 0 & 0 & 0 & 0 & \underline{0} & 0 & 0 & 0 & 1 \end{array} \quad \rightarrow \quad \begin{array}{cccccccccc} & 1 & 1 & 1 & ? & 1 & 1 & & & \\ & 1 & 0 & 1 & 0 & 1 & 0 & & & \\ 1 & 0 & 0 & 0 & \underline{0} & 0 & 0 & 1 & & \end{array} \quad \rightarrow \quad \begin{array}{cccccccc} & 1 & 1 & 1 & 1 & & & \\ & 0 & 1 & 0 & 1 & & & \\ 1 & 0 & 0 & \underline{0} & 0 & 1 & & \end{array} \quad \rightarrow \quad \begin{array}{cccc} & 1 & 1 & \\ & 1 & 0 & \\ 1 & 0 & \underline{0} & 1 \end{array}$$

Let F^1 be the set of sites at least distance 4 away (in the neighborhood graph) from all 1's generated by the downward EBD. Further, assume that A_0 is positioned so that, of the 1's with largest y-coordinate, the rightmost is at 0 and the leftmost is at $-L$. Let

$$F_t^2 = \{(x,y) : 0 \le y \le t-2, -y-L \le x \le y\}.$$

Then the argument so far implies that

$$F^1 \cap F_t^2 \subset A_t,$$

and therefore

$$F^1 \cap F_\infty^2 \subset A_\infty.$$

Arguments in Section 7 now imply that $|A_\infty^c \cap [-2^n, 2^n]^2| = \mathcal{O}((1+\sqrt{5})^n)$, and therefore the asymptotic density is 1. □

We do not know whether there are seeds that generate a number of 0's on the order of the fractal upper bound $(1+\sqrt{5})^n$ in Theorem 4. It is easy to check that a pair of diagonally adjacent sites leaves on the order of 2^n holes in $[-2^n, 2^n]$.

Even from simple seeds which result in a replicating EBD, Packard *Box* rules not covered by Table 2 or one of our theorems appear to generate complex growth within web walls. Semiporous EBD boundaries lead to intricate feedback effects such as delayed nucleation from concave exterior corners of the crystal and irregular timing of the final stages of fixation. The reader is encouraged to simulate, from a singleton, *135*, *157*, and especially *14*, as representative examples. Such phenomena serve to highlight the fine line between solvable and intractable Packard snowflakes.

References

[**BDR**] C. D. Brummitt, H. Delventhal, M. Retzlaff, *Packard snowflakes on the von Neumann neighborhood*, Journal of Cellular Automata 3 (2008), 57–80.

[**Epp**] D. Eppstein, *Cellular Automata: Replicators*. `http://www.ics.uci.edu/ eppstein/ca/replicators/`

[**Eva**] K. M. Evans, *Replicators and Larger than Life examples*, in "New Constructions in Cellular Automata," eds. D. Griffeath and C. Moore, Oxford University Press, 2003, pp. 119–159.

[**GG1**] J. Gravner, D. Griffeath, *Cellular automaton growth on $\mathbb{Z}^2$: theorems, examples and problems*, Advances in Applied Mathematics 21 (1998), 241–304.

[**GG2**] J. Gravner, D. Griffeath, *Modeling snow crystal growth I: Rigorous results for Packard's digital snowflakes*, Experiment. Math. 15 (2006), 421–444.

[**GG3**] J. Gravner, D. Griffeath, *Modeling snow crystal growth II: A mesoscopic lattice map with plausible dynamics*, Physica D 237 (2008), 385–404.

[**GG4**] J. Gravner, D. Griffeath, *Modeling snow-crystal growth: A three-dimensional mesoscopic approach*. Physical Review E 79 (2009), 011601, 1–18.

[**Gra**] J. Gravner, *Growth phenomena in cellular automata*, In "Encyclopedia of Complexity and Systems Science," ed. R. A. Meyers, Springer, 2009.

[**Gri**] D. Griffeath, *Primordial Soup Kitchen*. `http://psoup.math.wisc.edu/extras/1ormore/1ormore.html`

[**Jen1**] E. Jen, *Exact solvability and quasiperiodicity of one-dimensional cellular automata*, Nonlinearity 4 (1991), 251–276.

[**Jen2**] E. Jen, *Transience and dislocations in one-dimensional cellular automata*. In "Cellular automata and cooperative systems (Les Houches, 1992)," NATO Adv. Sci. Inst. Ser. C Math. Phys. Sci., 396, Kluwer Acad. Publ., 1993, pp. 299–310.

[**MW**] R. D. Mauldin, S. C. Williams, *Hausdorff dimension in graph directed constructions,* Trans. Amer. Math. Soc. 309 (1988), 811–829.

[**NN**] G. Nicolis, C. Nicolis, "Foundations of Complex Systems." World Scientific, 2007.

[**Pac**] N. H. Packard, *Lattice models for solidification and aggregation*, Institute for Advanced Study preprint, 1984. Reprinted in "Theory and Application of Cellular Automata," ed. S. Wolfram, World Scientific, 1986, pp. 305–310.

[**PW**] N. H. Packard, S. Wolfram *Two-dimensional cellular automata*, J. Statist. Phys. 38 (1985), 901–946.

[**TM**] T. Toffoli, N. Margolus, "Cellular Automata Machines." MIT Press, 1997.

[**TR**] A. Trevorrow, T. Rokicki, *Golly*. `http://golly.sourceforge.net/`

[**Wil1**] S. J. Willson, *Cellular automata can generate fractals,* Discrete Appl. Math. 8 (1984), 91–99.

[**Wil2**] S. J. Willson, *Computing fractal dimensions for additive cellular automata,* Phys. D 24 (1987), 190–206.

[**Woj**] M. Wójtowicz, *Mirek's Cellebration: a 1D and 2D Cellular Automata explorer*. `http://mirekw.com/ca/`

[**Wol1**] S. Wolfram, *Computer software in science and mathematics*, Scientific American 251 (September 1984), 188–203.

[**Wol2**] S. Wolfram, "A New Kind of Science." Wolfram Media, 2002.